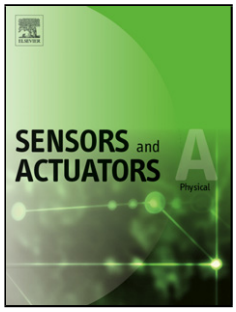

Title: Theory, Technology and Applications of Piezoresistive Sensors: a Review

Authors: A.S. Fiorillo, C.D. Critello, A.S. Pullano

PII: S0924-4247(18)30843-4
DOI: https://doi.org/10.1016/j.sna.2018.07.006
Reference: SNA 10871

To appear in: *Sensors and Actuators A*

Received date: 22-5-2018
Revised date: 27-6-2018
Accepted date: 2-7-2018

Please cite this article as: Fiorillo AS, Critello CD, Pullano AS, Theory, Technology and Applications of Piezoresistive Sensors: a Review, *Sensors and Actuators: A. Physical* (2018), https://doi.org/10.1016/j.sna.2018.07.006

Review Article

Theory, Technology and Applications of Piezoresistive Sensors: a Review

A.S. Fiorillo[a*], C.D. Critello[a§], A.S. Pullano[a§]

[a]Department of Health Sciences, University Magna Graecia of Catanzaro, Catanzaro, Italy

* Corresponding Author:
Prof. Antonino S. Fiorillo
nino@unicz.it

[§]Contributed equally to the manuscript

Abstract

Sensors based on the detection of small resistance variations are universally recognized as piezoresistive. Being one of the simplest, most common and most investigated classes of sensors, continuous efforts are focused on creating improved devices with higher performance that can be used in many commercial and non–commercial applications (e.g. evaluation of strain, pressure, acceleration, force etc.). Consequently, despite the fact that more than 150 years have passed since the discovery of the piezoresistive effect in some classes of metals and semiconductors, the development of such sensors remains interesting and topical. Moreover, with the advent of second–generation robotics, research on piezoresistive sensors has undergone a massive increase. This paper aims to be a short, self–consistent vademecum which would be useful to researchers and engineers, since it focuses on the fundamentals of theory, materials, and readout–circuit design pertinent to the most recent developments in the field of piezoresistive sensors.

Abbreviations

A	Area
a	Lattice constant
A_{CM}	Common mode gain
A_d	Differential gain
B	Conductivity factor
$CMRR$	Common Mode Rejection Ratio
D	Beam length
E	Energy
$\mathcal{E}$	Electric field
F	Force
GF	Gauge factor
h	Planck's constant
I	Inertia
$\mathfrak{I}$	Electric current
k	Wavenumber
l	Length
L	Quantum well width
m	Mass
m^*	Effective mass
n	Principal quantum number
p	Particle momentum
q	Electron charge
R	Electric resistance
s	Stress
T	Temperature
t'	Scattering mean time
U	Potential energy
V	Volume
v	velocity
W	Width
X	Volume fraction
α	Temperature coefficient
α_i, β_i, γ_i	Direction cosines
δ	Displacement
ε	Strain
η	Elasticity
ϑ	Resistance variation
μ	Charge mobility
ν	Poisson’s ratio
π_{ij}	Piezoresistive coefficient
ρ	Resistivity
σ	Conductivity
σ_l, σ_t	Longitudinal, Transverse stress

τ	Torque
Ψ	Wave function
ψ_n	Time–independent wave function
ω	Angular velocity

Keywords

Piezoresistance; piezoresistive devices; sensors; strain; pressure gauges; metals; semiconductors; polymers; micromachining; electronic circuits; thick film sensors; thin film sensors; tactile sensors.

1. Introduction

Piezoresistive sensors base their operating principle on the piezoresistive effect experienced by some classes of materials upon elastic deformation. Universally recognized as the most widely–used devices on both micro– (integrated devices, microelectromechanical systems "*MEMS*", etc.), and macro–scales (e.g. single sensors, arrays of sensors) their scientific interest is attested to by the increasing number of scientific publications involving piezoresistivity, the trend of which is shown in Fig.1. A more comprehensive analysis of the literature shows that piezoresistive sensors, even those embedded in sophisticated electronic devices, have been very pervasive in different fields (e.g. biological and biomedical applications, harsh environments, heavy industry).

The application of piezoresistive sensors has progressed enormously in the well–known field of robotics in its more general sense, as will be emphasized in this review [1, 2]. In the latest literature, many efforts have been focused on the integration of such sensors in biomedical robotics for tactile perception and for the development of the so–called "*electronic skin*" (e–skin) [3, 4] in addition to grasping [5, 6], and use in exoskeletons and artificial limbs [7]. Nevertheless, in the field of advanced robotic tactile sensors piezoresistive materials have been in constant competition with piezoelectric materials since the 80's [3, 4, 8, 9].

This paper is organized with the first part focused on the background of piezoresistivity in metals and semiconductors in order to highlight the different origins of the piezoresistive effect. Then a section follows which is dedicated to the transducers based on both the geometrical and the physical piezoresistive effect with particular emphasis on the adopted

materials, technological solutions, and applications. Finally, a section is dedicated to the most recent advances in the design of the readout of electronic circuits.

2. Piezoresistivity

The discovery of piezoresistivity dates back to 1856, and is attributed to Lord Kelvin (Sir William Thomson, Belfast, 1824–1907) [10, 11]. A step forward in the development of piezoresistive devices was made with the discovery of the piezoresistive effect in Silicon (*Si*) and Germanium (*Ge*) in 1954. The contribution of integrated–circuit (IC) technology led to the development of the first generation of commercial Si strain sensors, *strain gauges* (sometimes referred to as *strain gages*) in the late 1950s (although both spellings exist, the word *gauge* appears to be a more appropriate term to identify a device used in sensing and measurement) [12–14]. After World War II, the adoption of such devices began to open up new scenarios in emerging fields such as robotics, with the first examples of tactile sensors, favoring the birth of new classes of materials that fit the various requirements (e.g. piezoresistive silicone rubber for the fabrication of conformable devices and the use of silicon carbide for high–temperature applications) [15–17].

The etymology of the composite word "*piezoresistive*" includes two words of different linguistic origin: "piezo", from the Greek "*piezein*" (πιε΄ξω, infinitive πιε΄ξειν) which means «to press, to compress», and is common to other similar effects such as the piezoelectric effect, and "*resistive*", from the Latin "resistĕre" which means, «to stop». Although the physical nature of the energy transduction phenomenon is different, the term was coined in analogy to the piezoelectric effect. By referring to the electric nature of the devices that we shall describe, and to the etymological meaning of the word "*piezoresistive*", we may argue that such an effect involves a change in the resistance R of an electric conductor ($R=\rho \cdot l/A$), where ρ is the material resistivity [$\Omega \cdot cm$], l the conductor length, and A the transverse section area, because of a change in its geometrical parameters originated by an external stimulus (at the macroscopic level). However, in certain materials, an equally important part of the piezoresistive effect is due to the change in the resistivity ρ [12, 18]. While important studies were focusing on semiconductor materials which exploit the energy band theory, investigation was starting on a new class of composites consisting of conducting particles dispersed in an insulating matrix [19, 20].

Differently from piezoelectric materials, piezoresistive materials are not inherently able to generate an electric signal when strained, while piezoelectric materials spontaneously generate an electric potential difference. The former needs to be supplied by an external voltage source. If a voltage is applied between the extremities of a conductive bar, the geometry of which undergoes a deformation as a consequence of the exerted forces, the current also changes according to the change in the resistance, as Ohm's law states. The current that flows through the bar is directly related to the external stimulus (in other words resistance varies in relation to the mechanical input signal). Piezoresistive sensors are generally defined as "*active sensors*". These, of course, are different from "*passive sensors*", which spontaneously generate an electric signal when stimulated so they do not need to be supplied by an external voltage source [21]. Contrarily, active sensors need specific supply circuits depending on the technology of the transducer. Piezoresistive sensors are also used to perform direct measurements of dynamometric and geometric parameters. These may include force (friction, Coriolis, etc.), displacement, deformation, mass, pressure, flow, level, height, torque, acceleration, cracks, creep, and fatigue [22–28]. Very different materials, such as conductive elastomers, carbon fibers, and pure metals or alloys — commonly nickel and copper — are involved in the technological processes for the manufacturing of piezoresistive sensors. More sophisticated processes are based on thin–film–, thick–film– and solid–state technologies [29, 30].

3. Piezoresistive effect in metal conductors

Let's consider an isotropic electrically conductive, cylindrical bar (see Fig. 2a), to which an electric field $\mathcal{E}$ is applied longitudinally. Assume that R is its resistance in the quiescent state, at room temperature. Let us now suppose that, upon elongation, because of an applied tensile force F, the initial value of the piezoresistor, R_0, changes to the final value R. Through differentiation of the expression

$$dR = \frac{\partial R}{\partial \rho} d\rho + \frac{\partial R}{\partial l} dl + \frac{\partial R}{\partial A} dA$$

and dividing by R we finally obtain

$$\frac{dR}{R} = \frac{d\rho}{\rho} + \frac{dl}{l} - \frac{dA}{A}. \qquad (1)$$

Therefore, the initial value of the length (l_0) the diameter (d_0) and the resistivity (ρ_0), after deformations reach the final values of l_1, d_1 and ρ_1.

We define the "*longitudinal strain*" $\varepsilon_l = \mathrm{d}l_0/l_0$ as the variation in length per unit length and the "*diametral strain*" $\varepsilon_d = \mathrm{d}d_0/d_0$ as the variation in diameter per unit diameter. Because of the increase in length, a reduction in the cross–sectional area occurs too, ruled by Poisson's ratio $\nu = \varepsilon_d/\varepsilon_l$ (diametral strain per longitudinal strain). Hence, after the application of a tensile strain, the final length and diameter are respectively given by $l_1 = l_0(1+\varepsilon_l)$, and $d_1 = d_0(1-\varepsilon_d)$ while the new cross–sectional area is $A = \pi(d_0/2)^2(1-\varepsilon_d)^2$. Usually the strain is expressed in microstrain, με, as the ratio of 10^{-6} of length unit to the same length unit. Suppose now that there is also a change in volume during the deformation; the incremental variation is $\mathrm{d}V_0 = A_0\,\mathrm{d}l_0 + l_0\,\mathrm{d}A_0$ where V_0 and A_0 are the volume and the cross sectional area, in the quiescent state, respectively. On the other hand $\mathrm{d}V_0 = V_1 - V_0 = A_1 l_1 - A_0 l_0$ from which:

$$dV_0 = \pi\left(\frac{d_0}{2}\right)^2 (1-\varepsilon_l\nu)^2 l_0 (1+\varepsilon_l) - A_0 l_0 \tag{2}$$

By developing the square in brackets $(1-\varepsilon_l\nu)^2$, and neglecting higher order infinitesimals we have

$$dV_0 \cong A_0 l_0 \varepsilon_l (1-2\nu)\,. \tag{3}$$

By considering Eq. (3), with $\varepsilon_l = \mathrm{d}l_0/l_0$ and following the substitution in Eq. (1) for which l, A and R, have been used in place of l_0, A_0 and R_0, we finally obtain:

$$\frac{dR}{R} = \frac{d\rho}{\rho} + \frac{dl}{l}(1+2\nu)\,. \tag{4}$$

Now we can define the longitudinal gauge factor GF_l, as the ratio of the change in R compared to the relative change in length l

$$GF_l = \frac{dR/R}{dl/l} = \frac{dR/R}{\varepsilon_l} \tag{5}$$

and by substituting Eq. (4) into Eq. (5) we can write

$$GF_l = 1 + 2\nu + \frac{1}{\varepsilon_l}\frac{d\rho}{\rho}\,. \tag{6}$$

In most practical cases, however, the strain gauges have a planar geometry with a thickness *t* much smaller to the length *l* and the width *W*. If an electric field $\mathcal{E}$ is now applied to a planar strain gauge along the transverse direction w orthogonally to the applied force *F* (out of the page in Fig. 2b), the conducting material experiences the so–called "*transverse piezoresistive effect*". The aforementioned analysis applies in this case too, and we speak of the transverse gauge factor GF_t. Table 1 gives the resistivity and longitudinal gauge factors of the most common metals used in piezoresistive sensor fabrication.

4. The Piezoresistive Effect in Semiconductors

Piezoresistive effect in semiconductors, which manifests itself at the atomic level is less evident but much more important than the purely geometrical effect, and contributes to the dependence of the resistance variation on the strain.

This effect, discovered by Smith [12], is based on the induced stress modulation of the electric field generated by the charge transport. It is typical of elastic semiconductor bodies, such as silicon, germanium and gallium arsenide, and leads to substantial differences in the gauge factor previously introduced in Eq. (6). The piezoresistive effect may now be studied on the basis of the semiconductor theory or of a phenomenological development. Our discussion is based on the former theory while the phenomenological aspect will be briefly outlined, since an exhaustive explanation may be found in [36]. By rewriting the expression of the electric resistance as a function of the conductivity of the material, $\sigma = qn\mu$, where *n* is the electron concentration, Eq. (l) and Eq. (4) may be rewritten and, after substitution in Eq. (5) we obtain

$$GF = 1 + 2\nu - \frac{1}{\varepsilon}\frac{d\sigma}{\sigma} = 1 + 2\nu - \frac{1}{\varepsilon}\frac{d(n\mu)}{n\mu}, \tag{7}$$

which applies for both the longitudinal and transverse strains. In semiconductors, the gauge factor *GF* is primarily due to the high contribution of the changes that occur in the conductivity σ, or equivalently the resistivity ρ, since the geometrical part gives approximately the same contribution that we have found for metal strain gauges. As stated in Eq. (7), the changes in conductivity (resistivity) are related to the change in the number of free electrons and the change in mobility induced by the lattice deformation. Indeed, in

crystalline semiconductors the longitudinal and transverse gauge factors may be strongly influenced by the doping level, type, and the crystallographic direction along which the tensional or compressional stress is applied [36].

4.1 Energy band theory

The total energy of a particle (with mass m and velocity v), according to classical mechanics, is given by the sum of the potential energy of the particle U, and its kinetic energy $p^2/2m$ ($p = mv$ is the particle momentum). By using abstract quantum mechanical operators, the time–independent Schrödinger equation is given by

$$-\frac{\hbar}{2m}\frac{\partial^2\psi(x)}{\partial x^2} + U(x)\psi(x) = E\,\psi(x) \tag{8}$$

The separation constant E corresponds to the energy of the particle (for a particular solution to the above equation, E_n corresponds to the time–independent wave function ψ_n). In addition, for a particle trapped in an infinite square well (in the one–dimensional problem $U(x) = 0$ when $0<x<L$, $U(x) = \infty$ when $x=0; L$), the above equation assumes the form of the wave equation for a free particle. However, if the potential at the boundaries of the well has a finite value $U_0 > E$, the boundary conditions do not force the wave function $\psi(x)$ to be zero at the barrier, neither within the barrier, nor on the other side. There is a probability of finding the particle outside of the well, although its energy is less than the potential barrier V_0 (tunneling effect). The energy of the particle trapped in the potential well is quantized and its expression is given by

$$E_n = \frac{n^2\pi^2}{2m}\left(\frac{h}{2\pi}\right)^2\frac{1}{L^2} \tag{9}$$

in which $n = \pm1, \pm2, \pm3,...$, is called the quantum number. The negative values for the quantum number are redundant and the unique solutions are related to positive values of n. Each energy level E_n of the particle corresponds to a time–independent wave function ψ_n. By defining the wave number as $k=n\pi/L$, (9) becomes

$$E_n = \frac{k^2}{2m}\left(\frac{h}{2\pi}\right)^2 . \tag{10}$$

The energy of an electron, which moves in a single crystal semiconductor (i.e. a periodic structure with a lattice constant "a") because of the interaction with the atoms of the lattice,

may assume only certain values, while others are not allowed. This situation, compared to that of a free electron in a vacuum, is depicted in Fig. 3a. The forbidden energy bands occur around $k = n\pi/a$, while, far from these values, in the allowed bands the electron behaves as a free particle. The energy plot $E(p)$ of a free electron partially overlaps the energy plot $E(k)$ of an electron which moves in solids. The key point of piezoresistivity in semiconductors lies in the modification of the energy gap (the upper and lower values are defined for each $k = n\pi/a$) as a result of volume changes under the applied stress. However, the piezoresistive effect cannot be explained, in a very simplistic manner, on the basis of the one-dimensional case we have just discussed.

In order to clarify how it occurs in crystal semiconductors (the general treatment is described by Bloch theory) we need to approach the entire problem by considering the three–dimensional (x,y,z) model known as the many–valley energy band model. From the mono–dimensional problem, after simple mathematical manipulation we obtain two different expressions for the electron mass:

$$m = \frac{1}{d^2E/dp^2}, \qquad m^* = \frac{\hbar^2}{d^2E/dk^2} \tag{11}$$

in which quantum mechanics defines m^* as the electron effective mass. Figure 3b shows the second derivative of E versus both p and k in (π/a, $2\pi/a$). For a free electron, d^2E/dp^2 is constant and positive. However, for an electron in a periodic lattice d^2E/dk^2 is not constant and, in addition, it is negative at the top of the band. Hence, the effective mass $m^*<m$, at the bottom of the band, and $m^*>m$, at the top of the band, where the effective mass is also negative. The result is that when an electric field is applied, the electrons at the bottom and the top of the band move in opposite directions. For completeness, this fact must be considered along the three crystallographic directions x,y,z. Along these directions quantum mechanics associates different wave numbers k_1, k_2, k_3 to the components of the electron motion, so m^* is strictly related to the direction of the motion of the electron in the crystal lattice.

The effective mass is related to the mobility μ_n of an electron (which we have already introduced for metal strain gauges) by $\mu_n = qt'/m^* = v/\mathcal{E}$ where t' is the mean time between scattering events in the lattice [37]. For this reason, we must expect that mobility will also be affected by the direction of the motion of the electron in the lattice. This is shown in

Fig. 4 where the constant energy surface near the minima, in the conduction band, are also reported in the three–dimensional case, for *Ge*, *GaAs*, and *Si*. The mobility along the principal axis of the constant energy surfaces, which have an ellipsoidal shape for *Si*, is quite different from that along the secondary axis (see Fig.4c). When we modify the lattice spacing by applying an external stress, we modify the energy levels as well (dashed lines).

When *n–Si* is under tensile stress along the [100] *k*–direction — longitudinal effect — the minimum energy level increases along that direction while it decreases along the other two. The opposite occurs under compression along [100] — transverse effect. In the latter case, the stress can break the equivalence of the minima, resulting in shifting upward and downward in energy. Electrons will then be transferred to the lower lying minima to minimize the free energy. Thus, mobility decreases and, as a result, the resistivity increases.

Under certain conditions, the electrons in the valence band might also contribute to conductivity in semiconductors. The phenomenon may be better understood by considering the unoccupied states in the valence band referred to as holes. Since holes have a positive charge, under an electric field, they move (within the valence band) in the opposite direction from electrons (which move within the conduction band). There is no net current in the valence band unless at least one electron is removed. However, as for *n–type* semiconductors only the electron contribution is important, while for the conduction process in *p–type* semiconductors only the contribution of hole motion in the valence band is relevant. In contrast to n–Si, we now have two different energy functions *E(k)* which correspond to two different energy bands. Hence, the second derivative of *E* with respect to *k* has two different values in the same *k* direction which lead to two different effective masses and mobility values. The difference between the two masses and mobility, respectively associated to the two different energy bands, increases in the [111] direction which, for this reason, is the most sensitive to stress application.

If we now apply a traction to the *p–Si* along the [111] direction, the two bands split apart from each other and the respective hole populations change, since holes— which lose energy— move to the top where they have decreased mobility, resulting in "*heavy holes"*; the "*light hole*" band lowers with respect to the former one (see Fig. 5).

As the hole population with decreased mobility increases (the average hole mobility μ_p decreases), the conductivity $\sigma_p = qp\mu_p$ decreases and consequently the resistivity increases

[38]. In contrast to *n-type* silicon, which has a negative gauge factor of about –135, Smith found a positive gauge factor of up to 175 in *p–type Si* massive bodies [12]. Another important consideration concerns the doping level in both cases; indeed, as regards low–impurity concentrations, the percentage of carriers which moves to lower energy levels is larger as compared to that of highly–doped silicon. The consequence is that low–doped materials have a high gauge factor.

4.2 The phenomenological approach

On the basis of the phenomenological development in three–dimensional space, the relative resistance change may be expressed as a function of the longitudinal and transverse piezoresistive coefficients [36]. The electric field vector, $\mathcal{E}$, is related to the current vector, $\mathfrak{I}$ by Ohm's law $\mathcal{E} = \rho\,\mathfrak{I}$, through the resistivity tensor ρ (a 3x3 matrix). In crystal having a cubic structure, such as *Ge, GaAs,* and *Si* the number of the resistivity matrix elements is reduced to three ($\rho_1, \rho_2, \rho_3 = \rho$) by symmetry, which in piezoresistive materials depends on three normal and three shear–stress components. From the phenomenological point of view, the piezoresistive effect may be described by relative resistivity changes $d\rho/\rho$ now related to the stress components by a 6x6 matrix of π_{ij} elements called piezoresistive coefficients [Pa^{-1}]. When the symmetry is cubic, the number of independent piezoresistive coefficients is reduced to three: π_{11}, π_{12} and π_{44}. The longitudinal and transverse piezoresistive coefficients may now be expressed as

$$\begin{aligned} \pi_l &= \pi_{11} - (\pi_{11} - \pi_{12} - \pi_{44})\left(\alpha_1^2\beta_1^2 + \alpha_1^2\gamma_1^2 + \beta_1^2\gamma_1^2\right) \\ \pi_t &= \pi_{12} - (\pi_{11} - \pi_{12} - \pi_{44})\left(\alpha_1^2\alpha_2^2 + \beta_1^2\beta_2^2 + \gamma_1^2\gamma_2^2\right) \end{aligned} \tag{12}$$

in which α_1, β_1, γ_1 are the direction cosines along the longitudinal axis of the body with respect to cubic axis (the same as cubic axis and current flow), while α_2, β_2, γ_2 are the direction cosines along the transverse axis of the resistor [39]. Longitudinal and transverse piezoresistive coefficients are very important parameters in long resistor semiconductor design since they relate the relative change in resistivity to the applied stress

$$\frac{d\rho}{\rho} = \pi_l\sigma_l + \pi_t\sigma_t \tag{13}$$

in which σ_l and σ_t now represent stress, not conductivity. The direction of diffused or ion–implanted resistors with respect to crystallographic direction, when properly chosen in a

bridge configuration, allows us to sense only stresses applied in preferential directions. Usually, *p*–silicon is preferred for the making of semiconductor strain gauges since both longitudinal and transverse piezoresistive coefficients have a maximum in the <110> direction while *n*–silicon has a minimum in that direction [39].

Micromachined semiconductor piezoresistive devices and integrated circuit technologies allow the making of micro–sensors and micro–actuators for working at temperatures under 120 °C. The extreme ease with which it is now possible to etch very thin semiconductor cantilevers, allows the making of monolithic devices for both pressure and acceleration measurements.

A different class of new semiconductors—specifically, Silicon carbide (SiC)—has been extensively investigated for the fabrication of high–temperature devices [40–42]. In general, SiC have superior properties as compared to silicon in terms of elastic modulus, thermal conductivity, sublimation temperature, and chemical inertness. SiC forms stable polytypes (more than 200) which also influences the position of the conduction band minimum in the *k*–space. Thus, although briefly reported for completeness, the theory is limited only to Si while a more exhaustive treatment is available in the literature [43]. In Table 2 the longitudinal gauge factors of the most common semiconductors for piezoresistive sensor fabrication are reported. An important consideration concerns the influence of temperature because of changes in environmental conditions or piezoresistor self–heating. If the temperature changes from T_a to T_b, the resistance changes from R_a to R_b, given by

$$R_b = R_a[1 + \alpha (T_b - T_a)]. \tag{14}$$

Temperature compensation includes passive and active techniques. In the first case, extra components (e.g. fixed and temperature–dependent resistors) are used to compensate the errors of offset and sensitivity [44, 45]. Often the use of dedicated electronic circuits is necessary and these will be discussed in the section dedicated to readout–circuit design. Active techniques usually include digital compensation of the temperature and the use of additional temperature–monitoring units to reduce the above–mentioned errors in order to decrease, if possible, the incidence of temperature variations (e.g. digital calibration, thermostatic control) [46–48]. The gauge factor also changes with temperature, and there are substantial differences between the thermal expansion coefficients of the support (the

massive body being tested), the gauge, and the bonding material. There are gauges which self– compensate only for particular material supports; otherwise the effects of temperature must be electrically compensated [49, 50].

5. Piezoresistive Effect in Polymer Composites

Polymers are widely known as insulating matrices with excellent optical and mechanical properties. In the last 20 years many attempts to fabricate polymeric sensors by modifying their structure have been carried out. In the literature a great number of researchers have investigated the electric properties of polymers with incorporated particles (i.e. fillers) and the conduction mechanisms. The tool employed for the description of electric conduction in polymer composites (i.e. polymers and dispersed conductive particles) is called the *percolation theory*. At low filler concentrations (see Fig. 6a), metal particles are quite isolated and dispersed inside the insulating matrix resulting in a high electric resistance. By increasing the concentration of the filler, a conductive path is established and thus a drastic reduction in electric resistance comes about, defining the so–called "*percolation threshold"* (see Fig. 6b).

This is a simplified explanation but in reality different parameters are involved in the conduction mechanisms (e.g. particle geometries and properties, insulating matrix properties, and polymer–particle interaction). The conductivity of an insulating mixture above the percolation threshold can be expressed by using the model proposed by Kirkpatrick and Zallen as

$$\sigma = \sigma_0 (X - X_C)^B \tag{15}$$

where X is the volume fraction of the filler, X_C is the volume fraction of the filler when the percolation threshold is reached, and B the power of the conductivity increase after reaching the threshold. The latter is dependent on the properties of the filler (e.g. geometry) [54].

Several comprehensive and exhaustive reviews of different percolation models have been published, which even report on a wide range of supporting studies together with the experimental evaluations of the different polymers and fillers tested [54, 55]. When the

distance between the conductive particles is 10 nm or less but there is no physical contact, the tunneling conduction mechanism occurs, characterized by a power law current–voltage relationship [56, 57]. Conventional fillers used for increasing the electric conductivity of polymer composites are categorized as microfillers, the dimensions of which are in the microscale (e.g. carbon micro fibers, graphite), or nanofillers – e.g. carbon nanotubes (CNT), nanosheets of graphite/graphene, carbon black, etc. will be better discussed later.

6. Geometrical Effect–Based Strain Gauges

6.1 Non–Metal Strain Gauges

Conductive rubber and carbon–fiber strain gauges have been widely investigated in the field of robotics, particularly for the fabrication of tactile sensors. The goals were to achieve compliance, lightness, sturdiness, and low cost products; however both conductive rubber and carbon–fiber strain gauges suffer non–linearity and a high degree of hysteresis.

Conductive rubbers are usually fabricated by incorporating conductive particles of different types and dimensions, into a silicone–based matrix. Their sturdiness and compliance rendered them one of the most suitable materials for important applications in the field of robotics for the fabrication of tactile sensors able to withstand and adapt to damage and inaccuracy during robot positioning and the grasp. Row-by–column matrices are one of the most widespread configurations, an example of which can be seen in Fig. 7, fabricated with a Mylar film on silicone rubber.

In the literature, polyurethane foam has been investigated with an eye to increasing the compliance. The foam was coupled with conductive wires for the electric connections (made of conductive rubber) and a hybrid technology was realized [58]. The exertion of a force over the matrix causes variations in the contact area of the rubber sheets resulting in a variation of the electric resistance. At low loads the sensor response follows the law $R = k/F$ where constant k has the dimension of $\Omega \cdot kg$ and F is the applied force.

Different polymeric insulating materials have been adopted for non–metal strain gauges, such as polydimethylsiloxane (PDMS), polypropylene (PP), polycarbonate (PC), polymethyl methacrylate (PMMA), polyelectrolytes (PE), flexible epoxy and polyvinyl alcohol (PVA), to cite just a few examples [59–64]. Generally speaking, carbon is the most common filler used in polymer–based composites. The allotropic structures of carbon, such

as carbon nanotubes and graphene, have recently been investigated for piezoresistive–sensing applications. Graphene is a single–layered (one atom thick) two–dimensional array of carbon hexagons. First discovered in 1960 and later isolated in measurable quantities in 2004 by Geim and Novoselov, graphene has attracted quite lot of interest because it presents excellent mechanical, thermal and electric properties as compared to other conductive fillers [65–69]. Coskun et al. have proposed graphene–based elastomers as flexible polymer sensors with promising characteristics for detecting dynamic forces [70]. The inherent mechanical property of this new class of sensors to detect both small and large vibrations lies in its internal honeycomb–like structure, and it depends on the quantity of graphene used during the fabrication procedure [71]. Rinaldi et al. studied a novel lightweight piezoresistive sensor based on PDMS polymers in a foam format coated with multi–layer graphene nanoplatelets for applications requiring high sensitivity, such as wearable health care systems and human–machine interfacing devices [72]. Ye et al. investigated flexible and wearable strain sensors based on graphene oxide and polyethylenimine composites; these exhibited exceptional properties in terms of sensitivity, linearity, stretchabilty and durability [73].

Carbon nanotubes, first discovered by Iijima in 1991 and synthesized in 1993, have attracted a remarkable degree of interest as a possible filler material for the lightweight structures of polymers for numerous applications [74–77]. Unlike conventional strain sensors, (i.e. metallic and semiconductor) CNTs can be embedded into structural materials and can operate on a nanoscale as both multidirectional and multifunctional high–resolution sensors. Based on their structures, CNTs can be classified as single– or multi–walled, referring to the numbers of layers a CNT consists of Polymers in conjunction with CNTs have been used in many applied fields. A carbon nanotube–polydimethylsiloxane (CNT–PDMS) device has been developed for electronic skin applications in order to mimic the complex anatomical structure of the fingertip [77]. Yamada et al. presented a novel stretchable sensor for applications such as human motion detection, health monitoring, and rehabilitation. The device consists of aligned single–walled carbon nanotubes placed on PDMS substrates, and is able to detect strains 50 times greater than conventional metal strain gauges [78]. Cho et al. proposed three–dimensional nanoporous electrodes based on polymer substrates loaded with CNTs, achieving a gauge factor of up to 134 at a maximum

tensile strain of 40 %, and the potential applications of these could be the dynamic detection of human joint motion [77–81].

Basically, the piezoresistive properties of the conductive polymer composites are related to the type and the concentration of the filler that is added to the polymer matrix. Table 3 reports the resistivity values of a few conductive composites depending on the percentage content of the fillers used. As regards the gauge factor of conductive polymers loaded with carbon fillers, Shang et al. showed a non–linear behavior of the gauge factor as a function of the mechanical deformation for carbon black/silicone composites [82]. That result was different from that of other carbon–based polymers. For instance, Wang et al. reported a constant gauge–factor value for graphene/PDMS composites testing different filler concentrations [83]. A similar result was found for strain sensors made of CNT/PDMS composites [84].

Conductive polymer composites are commonly synthesized by mixing carbon fillers and polymer materials using low–frequency ultrasound with or without the addition of detergents [85]. This preparation method is quick and simple, overcoming limitations of metal and semiconductor systems. However, one of the main challenges is that it is usually difficult to homogenously distribute the carbon fillers within the polymer matrix [86]. Another drawback in the fabrication of conductive composites is the choice of the mix ratio of the carbon fillers and the polymer material. In fact, the mixing ratio determines the conductivity and the mechanical deformability of the conductive composites. High conductivity involves a reduction of stretchability, and this aspect has restricted the application fields of conductive composites especially as far as stretchable electronics is concerned [87].

6.2 Metal Strain Gauges

Undoubtedly, metal strain gauges are one of the most affordable and reliable technologies. The transducers are usually made using a metal strip several micrometers thick, patterned in a meandering geometry (see Fig. 8) to increase the length of the resistor over a small area (standard linear dimensions range from l mm up to a few cm). However, the width can be greatly inferior to the length *l* (see Fig. 8b). Thicknesses of about 5 μm are quite common resulting in a resting resistance which can range from 120 Ω to 750 Ω, even though transducers with larger values are also commercially available. In these cases,

the metal foil grid is set in a plastic or other type of support (paper, polyimide or other insulating polymers), resulting in an overall thickness of about 25 μm.

The temperature of operation of such devices can reach about 130 °C. The strain limit is about $40 \cdot 10^3$ με, while longitudinal and transverse gauge factors are about two and zero, respectively. However, the gauge factor also depends on the resistivity of the material $\rho = (qn\mu)^{-1}$. In metals, not one of these parameters is influenced by the experienced stress, (the reason for this has been previously discussed in section IV treating the piezoresistive effect of semiconductors).

Metal foil technology is well–suited to be mounted closely to the body which is subject to strain (these are often referred to as "bonded" strain gauges). Conversely, the so–called "unbonded" strain gauges are fabricated using different conducting wires and find different applications as force transducers. Bonded gauges are directly placed on the surface of the massive body, the strain of which must be measured. Because of its particular geometry, the piezoresistor is mounted with the grid parallel to the direction of the dominant strain "*longitudinal strain*" although the massive body may also experience a secondary "*transverse strain*", in the orthogonal direction; this, however, is totally neglected because of the null GF_t. Actually, the particular meandering geometry of bonded gauges makes them sensitive to transverse strain as well. However, the contribution of the very small parts of the conductor in a width–wise sense is negligible as compared to the contribution of the length–wise conductor. In Fig. 8c a geometrical arrangement of three strain gauges called a "*rosette*" is shown, for use in multi–component force fields.

Nanomaterials such as metallic nanowires have also been used for the design of piezoresistive sensors, especially for electronic skin applications. Different materials have been employed for the fabrication of nanowires [93–97]. Silver and gold nanowires have a high conductivity ($63 \cdot 10^4$ S/cm and $45.2 \cdot 10^4$ S/cm, respectively), ensuring low power consumption during the sensing operation [98]. However, they are expensive to fabricate. Copper nanowires present a conductivity ($59.6 \cdot 10^4$ S/cm) similar to that of nanowires made of silver or gold, but they are much cheaper to make. The main drawbacks related to the use of copper nanowires are the thermal oxidation and chemical corrosion that occur in harsh conditions, which leads to the loss of conductivity over time [99].

6.3 Thick–Film Strain Gauges

Strain gauges fabricated in thick film employ an organic fluid suspension made with conductive glass particles (i.e. resistive inks), deposited on a ceramic substrate (an alumina film 250–500 μm in thickness) [100].

In thick–film technology, the typical thickness that can be achieved is on the order of several microns up to several hundred microns, and this is strictly determined by the fabrication process [101]. Thick–film piezoresistive sensors are advantageous and are used in many applied fields, above all for their compatibility with difficult environments and their low fabrication costs [102–109]. Factors influencing strain sensitivity are the variations of resistivity, conductive–grain characteristics, the strain (e.g. elongation or compression) and the electric field. Although we have included thick–film strain gauges among those based on the geometrical piezoresistive effect, the conduction mechanism and the strain sensitivity are primarily dominated by the tunneling effect, which has been previously discussed in the semiconductor strain–gauge section. Typical thick–film longitudinal and transverse gauge factors are on the order of a few dozen, and find ample application in situations where there are high temperatures and harsh environments. At the moment thick–film technology, although inadequate for large–scale integration, is finding application in hybrid technology (e.g. assembled close to integrated circuits).

6.4 Thin–Film Strain Gauges

SnO and SiO cermet thin–films deposited onto ceramic substrates have been employed for strain gauge fabrication in the electronics industry [109]. Other types such as Ni and Ta may be deposited by means of vacuum processes, evaporation, sputtering or plasma–chemical vapor deposition. The miniaturization of these devices is both possible and economical, in particular when great accuracy is required [110]. The most common technological process of fabrication — particularly employed when accurate measurements are required — consists of sputtering the gauge material directly on top of the massive body being tested, and subsequently etching it according to proper geometries. The maximum operational temperature reaches about 150 °C [3].

Thin–film strain sensors have attracted a great deal of attention in a variety of applied fields, including electronic skin and health–monitoring systems. Metallic thin–film sensors using gold as the piezoresistive material are commonly used for measuring the tactile

sensitivity and forces exerted during the locomotion of small biological organisms [111]. In Xian et al. metallic–glass thin films are used as flexible strain sensors for electronic skin applications [112]. This material consists of different metals (zirconium, copper, nickel and aluminum) deposited on a flexible polycarbonate substrate. Engel et al. have developed an artificial skin that consists of a contact force and hardness–testing sensor based on a piezoresistive transduction mechanism. They fabricate their strain gauges using thin films made of nickel and chromium [113]. As compared to other thin–film strain gauges (CNTs, graphene, metals or alloys and conductive polymers), metallic–glass sensors combine advantages in terms of conductivity, flexibility, manufacturing costs, and sensitivity. In addition, metallic–glass strain sensors have shown very low temperature coefficient besides antimicrobial properties. All these properties make metallic glass a promising material, especially for electronic skin applications.

In the case of metallic thin–film sensors, the gauge factor is mainly based on geometric effects, and is about 2 [113]. The gauge factor is therefore comparable to that of metal strain gauges, but metallic thin–films have little stretchability, as do most metallic materials. In order to increase the stretchability of metallic thin–films, they are put onto polymeric substrates in curved or wavy shapes [114–116].

7. Piezoresistive Strain–Gauge Applications

7.1 Force sensors

Forces change the quiescent or motile state of a body to which they are applied. According to Newton's second law, under the application of a force $F = m\mathrm{d}v/\mathrm{d}t$, a body of mass m moves with an acceleration $\mathrm{d}v/\mathrm{d}t$. In the last 20 years, especially in the field of robotics, intensive efforts have been devoted to the development and sensorization of humanoids [117]. Contact sensors are of fundamental importance for the measurement of the physical forces that occur when a robotic end–effector makes contact with an object. In most of the recent literature having to do with robot sensorization, an approach based on the bio–inspired mechanoreceptor viewpoint (e.g. Merkel, Ruffini, Meissner and Pacini corpuscles) for tactile sensing is used [118, 119]. Each receptor is thus dedicated to a particular stimulus, such as static or non–static, which corresponds to the detection of static stress and vibrations [120]. Both as transducers and arrays, tactile sensors are required to

perceive an incipient stimulus, and to identify and detect the orientation/position of the target, giving exteroceptive information during its task [121]. A valid set of performance criteria that tactile sensors should have was suggested back in the 1980s and then progressively refined, as reported in Table 4.

More recently, the advent of the first and second waves of robotic systems for human mimesis and rehabilitation consequently changed the requirements in terms of piezoresistive sensor integration. Force measurements are usually performed by combining shear stresses with cantilever beams of different configurations [126].

Most commercial and non–commercial strain gauge sensors for force measurements are based on small deflections of beams, cantilevers or diaphragms [127–130]. Usually at least two or more gauges are bonded onto the opposite faces (top and bottom) of a cantilever or a membrane fixed at one or both ends, respectively. The need for flexible, compliant and conformable devices is accelerating their development in the field of composite materials as previously discussed, which combine mechanical flexibility and resistance and can protect the sensors from the external environment. Based on conduction mechanisms, the material/composites employed in tactile sensors can be further divided into strain gauges (e.g. metal– or silicon–based gauges), percolative (e.g. conductive rubbers, carbon–black– and carbon–nanotube–based composites), and quantum tunneling (thick film, metal dispersed particle–based sensors) [124, 131–133]. Recently, most of the commercial sensors dedicated to human touch mimesis are implemented with Force Sensing Resistors (FSR), consisting of conducting interdigitated electrodes deposited on a flexible polymeric film bonded on another conductive polymeric film. A spacer between the two films allows an electric contact to occur when a force is applied. These FSR are unusually employed in high–accuracy applications [7].

Concerning their functioning principle, in most of the integrated piezoresistive sensors, the force, applied at the end or in the central region, deflects the beam and induces a compression or an expansion of the gauges depending on the beam geometry and constraints. According to Hooke's law the modulus of elasticity $\eta = s/\varepsilon$, stress/strain, is given, for a traction F_T or compression F_C respectively, by

$$\eta_T = \frac{F_T / A}{\Delta L / L}, \qquad \eta_C = \frac{F_C / A}{\Delta L / L}. \tag{16}$$

The electric output signals of the gauges are proportional to the applied force through longitudinal displacement (see Fig. 9).

The major drawbacks of the classic (semiconductor and metallic) strain gauges are their mechanical fragility, and scarce thermal stability. In order to overcome these disadvantages, the use of flexible substrates was investigated both by integrating rigid transducers and/or by including microparticles in order to decrease the stiffness of the sensors.

A typical process for rigid transducer integration is the so–called Silicon–on–Insulator (SOI), in which an intermediate oxide layer is used to stop the etching of the bulk Si substrate (see Fig. 10a). The Si wafer is also oxidized on the bottom and a large window is subsequently opened. This opening serves to etch the bulk Si in the last steps. On the opposite side the silicon is etched away as far as the intermediate oxide stop layer, to form the cantilever. A new thin–oxide layer is grown as a passivation layer. Contact holes are opened in sequence, after which a thin metal (e.g. aluminum) layer is sputtered, patterned and etched in order to contact previously diffused resistors (see Fig. 10b). After protection of the top layer with insulating polymers, the bulk silicon is etched through the large window. Finally, the original oxide layer is etched and removed to form the cantilever (see Fig. 10 c, d).

7.2 Displacement sensors

Strain gauges mounted in order to sense both the tension and the compression of the beam are frequently used to make displacement sensors. A force sensor can be fabricated by a calibrated displacement sensor with a well–known stiffness. In Fig. 9b, the beam is deflected by a sensing shaft and the displacement can be measured using the following formula:

$$\delta = \frac{Fd^2(3D - d)}{6\eta I} \tag{17}$$

where D is the length of the beam, d is the distance at which the force F is applied, and I is the moment of inertia of the beam. Considering a given displacement at the center, the stress/strain is proportional to its thickness thus imposing constraints on the placement of the transducer element and the thickness of the beam [134]. Cantilevers and beams are

commonly designed and fabricated as displacement sensors using various topologies (see Table 5).

Working at low frequencies is important for reducing 1/f noise and even Johnson noise inherently due to thermal energy in the resistor. Long time stability (in terms of hours) is also desirable [138].

7.3 Weight sensors

One other application in which force transducers are used is that of weight measurements [139]. Weight can be seen as a particular force; more precisely it is the force which acts on any object immersed in a gravitational field. Hence, the weight measurement may be turned into a force measurement by taking into account the fact that the terrestrial gravitational field changes according to geographical characteristics. The gravitational acceleration decreases by about 0.53 % by moving from the poles to the equator and by about 0.03 % by moving from sea level to 1000 m [140].

7.4 Pressure sensors

Strain gauges for pressure measurements convert pressure variations (force per unit area) into resistance variations. Both bonded and unbonded metal strain gauges as well as sputtered thin film gauges have been used for this application. For measurements of the order of a few hundred kgm^{-2} semiconductor strain gauges are also used. The transducers are usually located on the backside of a membrane, opposite to where the pressure is applied.

The micromachining of silicon is currently a mature technology for the fabrication of pressure sensors although Si is easily broken (maximum strain of 2 %) [141]. This is a consolidated technology which makes the fabrication of devices possible that can sense a very wide range of pressures; this can be done by designing the transducer with the proper dimensions (e.g. diaphragm, beam, cantilever) [142]. The basic design structure among most types of pressure sensors is quite similar: a diaphragm, which flexes upon pressure, which is the parameter to be evaluated. Mechanical deflections/strains are thus transduced through properly located piezoresistive elements [143–145].

Notwithstanding the high gauge factor of the silicon–based pressure sensors, attention should be paid to the temperature coefficient of piezoresistivity (0.27 %·°C^{-1}) and doping

concentration, both of which impose limits on the temperature range and compensation circuits [146].

Although different canonical forms of integrated piezoresistors are often employed, Fig. 11 shows a typical arrangement of a cruciform pressure sensor.

7.5 Flow sensors

A particular application for pressure sensors concerns the indirect flow measurement of gasses or liquids. These sensors are classified as non–thermal devices, and the pressure variation due to variations in the flow of the substance is measured through a mechanical linkage between a diaphragm and the strain gauges.

The diaphragm, which is in direct contact with the fluid, converts a pressure variation into mechanical motion which is then accurately transmitted to a strain gauge bridge. When fluids are not highly corrosive, the strain gauge bridge is located directly on a membrane or a cantilever (see Fig. 12). Thin layers of insulating material are nevertheless used to prevent possible corrosion due to long periods of exposition to the fluid, short circuits due to fluid conductivity, or damage due to sensitivity to high temperatures.

Piezoresistive flow sensors have been applied in biomimetics, where the technology is used to mimic nature. Examples of flow biosensors can be found in vertebrates such as fish. These sensing elements consist of tiny structures known as hair cells, which are located in a well–organized manner on their bodies and act as flow sensors that monitor the surrounding environment for tasks related to motion, orientation and prey localization [147]. Invertebrates such as spiders also use hair cells as air–flow sensors to detect very slight displacements [148]. Recent studies have highlighted the role of hair cells in bat wings in connection with flight maneuverability [149]. Biological hair cells are also found in humans and other vertebrates for sensing acoustic vibrations and equilibrium [150]. Artificial biomimetic flow sensors based on the piezoresistive principle have been fabricated using different geometries and materials [151–154]. Shen et al. have exploited these sensing elements to fabricate piezoresistive flow sensors based on MEMS technology to measure the flow rate in the tubes used for intravenous infusion administration. The sensor is composed of a vertical hair located on a polymer diaphragm plus a gold thin–film that realizes the transduction [155].

A general drawback of the piezoresistive flow sensors is the mechanical damage induced by high flow velocities. Flow sensitivity and time response are the common parameters used to characterize this type of sensor, which are strictly related to the size of the cantilever used for the detection of the strain. Wang et al. reported that the flow–rate sensitivity of air flow sensors increases when wider cantilever beams are used. But the response time was found to increase as the cantilever width was decreased [156]. Data for piezoresistive flow sensors are reported in Table 6.

7.6 Torque sensors

Torque is the moment of a force applied to a body rotating around an axis in order to accelerate or decelerate its rotational motion. Hence, a torque transducer senses the shear stresses in a torsion bar, the axis of which rotates as a result of the applied torque. If F_t is the tangential force applied to a point far from the axis of a distance d, the torque is given by $\tau = F_t d. = I \cdot d\omega/dt$, where ω is the angular velocity. Usually bonded metal foil and semiconductor strain gauges in a cruciform arrangement (see Fig. 13), are used for this application. The strain gauges are placed at 45° angles relative to the main axis in order to maximize the sensitivity. One pair of sensors is designated for detecting tensional strains. The other pair can measure compressive strains.

Torque sensors are useful in many industrial applications, including robotics. For instance, these types of sensors have been used successfully in the rehabilitation field to support patients regaining mobility of the wrist joint [158]. Polymer–based composite materials have also been used to make piezoresistive torque sensors for implants and artificial joints, with the aim of increasing biocompatibility and compatibility with electronic circuitry while decreasing the manufacturing costs [159]. The use of piezoresistive torque sensors in robotic applications is still a question of compromise between sensitivity and torsional stiffness. In fact, these two factors are inversely proportional to each other. Moreover, other issues can be related to the placement of the strain gauges on the body of the sensors, and to miniaturization, although some advancements have been reported recently in terms of design optimization that aims at overcoming these drawbacks [160].

7.7 Acceleration sensors

Strain gauge sensors for acceleration measurements have the typical configuration of a force sensor terminating in a seismic mass. Accelerometers convert the alternating displacement of a mass–spring system (with dumping), around a quiescent position, into a variation of resistance. As in previously discussed sensors, acceleration measurements are performed by mounting two gauges on the opposite faces of a cantilever beam at the end of which a body of mass m is located (see Fig. 14). The damping medium is usually a viscoelastic fluid such as silicon oil (not shown in Fig. 14). The top and bottom strain gauges work alternately in tension or compression depending on the acceleration or deceleration (negative variation of body velocity) of the seismic mass. The mass is sensitive to orthogonal acceleration on the main surfaces of the cantilever, the displacement of which is proportional to the acceleration. Since *m* is known, the mass acceleration can be found by using Newton's second law $F=m\mathrm{d}v/\mathrm{d}t$. Devices are usually based on metallic bonded strain gauges as well as semiconductor strain gauges. The first silicon micromachined accelerometer was developed at Stanford University in 1979 [161]. The piezoresistor device is included within an electronic circuit that provides an electric signal linearly proportional to the acceleration. The whole system is only a few millimeters in size.

In accelerometer production, the etching process may be controlled in order to obtain the seismic mass at the end of the cantilever. When accelerated, the cantilever bends and the resistance values of the diffused piezoresistors change. The strain–sensing resistors are placed at points of maximum stress and the seismic mass may be suspended along one edge or from points along both edges.

Typical characteristics of piezoresistive accelerometers are frequency response, sensitivity (expressed in terms of mV/g), and linearity. More specifically, they have a broad frequency range (from dc up to a few kHz), a sensitivity of up to 25 mV/g depending on the gauge mounted on the cantilever beam, and a dynamic range of ±1,000g with an error of less than 1 % [162]. Other advantages are the low fabrication costs, the fact that it’s lightweight and the possibility of miniaturization. Notwithstanding the great sensitivity and good frequency response, piezoresistive accelerometers have some limitations such as the negative influence of high working temperatures on output performance, and the bandwidth that has to be traded off with sensitivity.

Acceleration sensors based on piezoresistive technology are widely used in the automotive, medical and robotics fields, as well as others [163]. An interesting use of piezoresistive accelerometers is related to the proprioception of robots, which provides information about their positioning and orientation [164]. Piezoresistive accelerometers are also used for measuring human tremors, a clinical manifestation characterized by involuntary movements of body parts [165]. The frequencies of neurodegenerative diseases — which are the cause of tremors — range from a few tenths of Hz up to 25 Hz, depending on the medical condition of the patient [166]. The good frequency response they give at very low frequencies together with their excellent sensitivity represent the main characteristics that legitimize the use of piezoresistive accelerometers in tremor diagnostic systems.

8. Electronic Circuits for Piezoresistive Devices

The electric output signal of a piezoresistive strain gauge in its original form is useless for practical purposes. Before further analog or digital conditioning, it needs to be amplified by low–noise circuits. The first stage of the electronic acquisition unit, the preamplifier, is the most important block since, in general, it matches two blocks of a different nature, the transducer itself and the global electronic circuit, made with other cascaded stages which are usually general purpose analog or digital circuits, and, less frequently, specialized circuits [167–169]. A classic conditioning circuit consists of a Wheatstone bridge through the generation of a non–zero voltage ΔV in response to bridge imbalance generated by one or more of the resistive elements (see Table 7).

Basically, the piezoresistive sensor consists of a Wheatstone bridge or a half–bridge circuit, the arms of which are made with dummy, R_D, and strain gauges, $R_G = R_D + \Delta R$, (the former are used for compensation purposes and are mounted onto the unstrained portion of the body being tested) [170]. Figure 15 shows a full Wheatstone bridge. There are four arms in which from 1 up to 4 strain gauges are connected to three, or fewer, dummy gauges.

Two nodes of the bridge are connected to the supply voltage *V*, while the other two are connected to the electronic preamplifier, mounted in the differential dc configuration, the output of which is related to the strain gauge resistance variation by

$$V_o = \frac{R_F}{R_D}\frac{\vartheta}{1+\vartheta}\frac{V}{R_D/R_F(2+\vartheta)/(1+\vartheta)}, \tag{18}$$

where ϑ *is* $\Delta R/R_D$. Apart from the full bridge configuration (i.e. load cell), resistive bridges suffer from an inherent non–linearity as long as $\Delta R/R_D$ <<1, in addition to the non–linearities arising from other sources.

The output–offset voltage, which may be of the same order of magnitude as the transduced signal and must therefore be compensated, is given by $V_{OS}=V_{io}(R_D+R_F)/R_D+(I_2-I_1)R_F$, where V_{io} is the input offset voltage of the operational amplifier, and I_1, and I_2 are the non–inverting and inverting input bias currents, respectively. For this preamplifier configuration, which has very low input impedance, an operational amplifier with a good common–mode rejection ratio, CMRR, is suggested. Figure 16 shows a better topology of the differential dc amplifier, where the output of the bridge (which, here too, may be made using from 1 up to 4 strain gauges) is connected to the so–called instrumentation amplifier [3, 167].

This topology, also known as a differential buffer amplifier, offers many advantages as compared to the former one. First of all it has very high input impedance. In addition, its gain may be easily changed by modifying the value of the resistor R_1. Then, if the second stage is carefully balanced, the preamplifier has a very high capability of rejecting common–mode (CM) signals. Indeed, since $V_{CM}=V_{01}=V_{02}$, the common–mode noise pickup is completely rejected by the second differential stage, which has a common–mode gain $A_{CM}=0$. The differential gain of the preamplifier is given by $A_d=1+2R_F/R_1$.

A third topology is sometimes used in combination with the half bridge. This is the simplest and least used circuit. However, for particular applications it has some advantages. The sensor consists of two arms which are respectively made using only one strain gauge and one dummy gauge in a potentiometric configuration (see Fig. 17) [171].

The bridge arms are connected to a current–to–voltage converter made with a low–noise operational amplifier. This configuration is suggested when the half bridge is connected

very closely to the converter. Indeed, in contrast to both the differential dc and buffer amplifiers, the CM signal is not rejected by the converter. Figure 18 shows another arrangement in which two similar configurations, if required, may be mounted on the opposite faces of a cantilever force sensor [3].

The strain gauge couple senses the pressure signals that have the same amplitude but are opposite in polarity. The push–pull voltages, due to a mechanical stimulus, may be added in modulus and amplified, if necessary, by a second differential stage. This circuit topology allows the doubling of the electric signal generated by the pressure on the cantilever and a drastic reduction in the noise generated by the transducers. As for the instrumentation preamplifier, the CM signal is now rejected by the second stage. The output of the upper or lower channel of the first stage does not depend on the strains induced simultaneously on both piezoresistor strain gauges, as would happen if a differential buffer amplifier was used. In the quiescent state, both the channels may be tested and calibrated separately. The gain is selected by using fixed resistors instead of variable resistors, which is preferable when the sensor is included in mobile small effectors. Finally, the sensitivity may be increased by increasing the bridge supply voltage. In contrast to the differential buffer amplifier, in this particular topology each operational amplifier of the first stage does not suffer from common–mode voltage limitation. The only limit in supplying voltage is imposed by the piezoresistive strain gauges because of self–heating, as well as the normal limitations of the gauge elements (4–5 V for most commercially available strain gauges). If ε_U and ε_L are, respectively, the strain on the upper and lower strain gauges, when an external force is applied to the cantilever (see Fig. 9a), the variations in the resistance of the upper and lower sensing elements are respectively $GF= \Delta R/R_U(1/\varepsilon_U)$ and $GF= \Delta R/R_L(-1/\varepsilon_L)$. Let V be the bridge supply voltage, R_F the feedback resistance of the current–to–voltage converter, and R_D equal to R_U, R_L, the resistance of the strain gauge in the quiescent state. Each converter output $V_0= -V(R_F/R_D)(\pm\Delta R/R_D)$ is proportional to the ratio $\pm GF\varepsilon$, where ε is the upper or lower strain. Moreover, the signal at the output of the differential dc amplifier is proportional to $GF\varepsilon_U - GF(-\varepsilon_l)$. The output offset voltage of each converter is given by the following expression $V_{OS}= -R_F\cdot(I_2+2V_{io}/R_D)$. In each of the analyzed configurations, temperature compensation may

be performed by inserting a resistor in series with the supply voltage or with a properly chosen arm of the bridge [52], [53].

Power consumption has become an important limiting factor in the development of piezoresistive sensors, especially if the power supply limits the design (e.g. wearable devices for biomedical and home applications) [172, 173]. In voltage mode readout circuits, a higher nominal value strain gauge yields lower power consumption while, for current mode circuit topology, the opposite happens [45, 172]. The effect of self–heating is the cause of frequent measuring errors unless the power is kept as low as possible [174]. Optimal length is often a compromise between the reduction of self–heating (shorter strain gauge) and the increase of the transverse loading factor (longer strain gauge) [53]. The typical power consumption of a resistive gauge element is in the mW range while for other technologies, such as that of piezoelectric or capacitive sensors, it can be reduced to a few hundred nW or less [175–177]. Compared to passive piezoresistors that need a voltage source to measure the strain, piezoelectric sensors generate an electric potential difference in response to a mechanical stimulus. Therefore, heating issues are limited since they do not require a power source to operate. Differently from metals and semiconductor–based piezoresistors, thin conducting polymers must be driven at sub–mW to avoid excessive self–heating due to the large temperature coefficient [178]. Being closely related to the material and size of the element, the ever–increasing need to scale down the device into the nanoscale range has emphasized the heating issue which is detrimental to noise and sensitivity [53, 179].

As previously highlighted in this section, while in the simplest cases piezoresistive sensors do not require complex conditioning circuitry, different strategies have been implemented for working under low–voltage/low–power conditions, at the same time increasing the accuracy that is also limited by errors of the electronic interface [180]. In the Wheatstone bridge, its greater sensitivity is paid by a higher excitation source, which limits its operation at low–power [180]. The effects of changes in the saturation current in a bipolar transistor (i.e. piezojunction) or in the p– and n–channel MOSFET (i.e. piezo–FET) current, both related to mechanical stress, have been investigated as a low– and ultralow–power alternative [182, 183]. In the latter cases, power can range from a few μW down into the nW range, even though the circuit complexity increases significantly [182–

184]. A number of techniques have been focused on an electronic interface for improving the overall performance of the sensor, including power consumption. A simple alternative, the so–called "*active bridge*", is based on the use of a current source for both biasing the gauge and amplifying the small output signal, allowing low–voltage operation and a consumption of only a few hundred μW [185, 186]. Moreover, interfaces with automatic compensation such as autozero circuits, chopper circuits and dynamic element–matching circuits have also been investigated as low–voltage, low–power integrated systems [180].

Integrated circuit technology offers the enormous advantages of combining both the micromachined transducer and the acquisition electronic unit in a monolithic device. Figure 19 shows a classical CMOS differential configuration used to amplify the output of on-Silicon Wheatstone Bridge. A few representative characteristics of an integrated CMOS amplifier are reported in Table 8, as found in literature for pressure sensors.

Alternative approaches have been more recently investigated using current–mode bridges which exploit the development of stable current sources and the second generation of current conveyors (CCII) [192, 193]. A current–conveyor–based interface offers advantages for the output signal (current) allowing us to disregard the effect of the relatively long wires used, and also enabling the evaluation of up to 5–decade electric resistant variations [194–196]. The concept of voltage/current–controlled negative resistances, also called Negative Impedance Converters (NICs), has come back into vogue because they grant low resistances in current sensing. In particular, the implementation of a negative resistance does not require extra temperature monitoring because it makes the output voltage insensitive to temperature [197, 198]. The literature reviewed in this section has been focused on the front-end interface that represents one of the core components of a complete device, which usually includes analog–to–digital conversion, signal processing, and communication modules. The latter should also exploit techniques to minimize the overall energy consumption, reducing the constraints on power supply with the aim of achieving higher efficiency in practical applications.

9. Discussion and Conclusion

The survey of the most recent developments in piezoresistive sensors cannot leave out the technological contexts within which they have been developed, and researchers have faced various challenges in this area. In spite of the fact that more than 150 years have passed since the first article on piezoresistivity appeared, and that much progress has been made in the field of integrated, flexible and even wearable piezoresistive sensors, some common points remain challenging.

After the first wave of metallic piezoresistive sensors appeared, it was clear to researchers that one of the main drawbacks was that undesirable physico–chemical and environmental effects (e.g. thermal oxidation and chemical corrosion) degraded the stability of the sensors over time [99]. In order to overcome these problems, investigations began in the 1980s on nanomaterial–based (e.g. zinc oxide nanowires) strain gauges, even though in some cases it was observed that their conductivity decreased with an increase in strain, limiting the use of these nanowires exclusively to low–strain applications [199]. Silicon–based nanowires, especially p–type, have also been widely investigated for piezoresistive sensing applications because they exhibit a very fine piezoresistive sensitivity (known as 'Giant Piezoresistance') as compared to bulk silicon, and they have been used mostly in mechanical sensing [200–204]. So the power of integrated–circuit technology made way for the fabrication of nanostructured semiconductor devices for the most varied applications, ranging from the evaluation of the contractile force of cardiomyocytes using a cantilever with a resolution of less than 0.1 nN, to the use of a gyroscope based on piezoresisistive nano–sensing for vestibular implant systems having the main advantage of low–voltage operation [205, 106]. In the same period of time, the revolution of sensors fabricated on flexible substrates came about simultaneously with the birth of flexible circuit technology which was crucial for innovative device fabrication methods [207]. Polymer–based MEMS technology is very flexible, highly compatible with biological systems and low–cost [208]. Many polymeric materials have been adopted for MEMS applications such as SU–8, polyimide, PDMS, PMMA and Parylene to name only a few.

The gauge factor was one of the key parameters for the classification of piezoresistive sensors. For instance, a GF of less than 10 identifies metal transducers while semiconductors exhibit a gauge factor of up to 200. The growing demand for mechanical flexibility due to the development of wearable electronics has led an ample use of polymer–

based conductive composites in sensing applications. This has had its pros and cons. For example, the increase in the use of polymer composites has upset the gauge–factor–based classification system. On the other hand, it has opened the doors to the investigation of materials with giant GFs (from GF <1 to ~ 10^3 or even greater), which allow new perspectives of application [73, 209, 210].

This review of the literature has highlighted the fact that piezoresistivity continues to remain one the most widespread phenomena for the design and fabrication of sensors for robotics and related fields. Although technology has made great strides forward, sensor design has remained anchored to the technological dogmas of the mid–1900s. Certainly, the advent of composite materials with their excellent characteristics has allowed researchers to overcome some problems related to the use of semiconductors and metals (see Fig.20), but other aspects require further investigation (e.g. stability and reproducibility) [211]. Table VIII shows some of the representative piezoresistive sensors that have been reviewed, the main physical, electric and metrological characteristics of which could be useful for a qualitative and quantitative comparison.

Apart from the variety of fields in which piezoresistive sensors are successfully employed, the challenge remains in robotic tactile–sensor manufacturing. Piezoelectric and capacitive sensors are the most recognized competitors of piezoresistors. On the basis of the bioinspired capabilities of humanoids, a distinction should be made between piezoresistive and capacitive transducers with respect to piezoelectric transducers. "....*the human sense of touch can be the starting point*...." [4]. Although outstanding progress has been made in the field of piezoresistive tactile sensors, the piezoelectric effect seems to be the best compromise for artificial tactile perception because of its strict similarity to the mechanoreceptors of bio–systems: that is, *Pressure difference = Current generation* [120, 212, 213]. On the other hand, in reference to the electric nature of piezoelectricity and piezoresistivity, the former doesn't imply the use of transducer supply voltage, as happens with active piezoresistive transducers, with enormous advantages in terms of dimension, circuit complexity, and power consumption, at least as far as humanoid artificial touch goes. However, a comprehensive approach results necessary to reduce power consumption in the μW range, which is a practical limit for most portable applications (e.g. biomedical) [214]. Even though the fragility of semiconductor strain gauges is a limiting factor in

robotic end-effectors, their superiority and reliability remains unquestionable in many industrial and research fields.

References

[1] R.D. Howe, Tactile sensing and control of robotic manipulation, *Advanced Robotics*, 8:3 (2010) 245–261.

[2] J. Tao, X. Yu, Hair flow sensors: from bio–inspiration to bio–mimicking—a review, *Smart Materials and Structures*, 21 (2012) 1–23.

[3] A.S. Fiorillo, A Piezoresistive Tactile Sensor, *IEEE Transactions on Instrumentation and Measurement*, 46:1 (1997) 15–17.

[4] R.S. Dahiya, G. Metta, M. Valle, G. Sandini, Tactile sensing: from humans to humanoids, *IEEE Transactions on Robotics*, 26 (2010) 1–20.

[5] M.R. Cutkosky, R.D. Howe, W.R. Provancher, Force and Tactile Sensors, In Springer Handbook of Robotics, Springer, New York, NY, USA, 2008.

[6] H. Yousef, M. Boukallel, K. Althoefer, Tactile sensing for dexterous in hand manipulation in robotics: A review, *Sensors and Actuators A: Physical*, 167 (2011)167–171.

[7] A. Damilano, A. Lince, S. Appendino, H.M. A. Hayat, P. Ariano, D. Demarchi, et al., Commercial tactile sensors for hand exoskeletons: practical considerations for ultra–low cost and very–low complexity read–out, *IEEE Instrumentation & Measurement Magazine*, 19:5 (2016) 49–56.

[8] A.S. Fiorillo, P. Dario, M. Bergamasco, A sensorized robot gripper, *Robotics and Autonomous Systems*, 4:11 (1988) 49–55.

[9] P. Dario, D. De Rossi, Tactile sensors and the gripping challenge: Increasing the performance of sensors over a wide range of force is a first step toward robotry that can hold and manipulate objects as humans do, *IEEE Spectrum*, 22:8 (1985) 46–53.

[10] W. Thomson, On the electro–dynamic qualities of metals: Effects of magnetization on the electric conductivity of nickel and of iron, *Proceedings of the Royal Society of London*, 8 (1856) 9546–550.

[11] J.W. Cookson, Theory of the piezo–resistive effect, *Physical Review Journal*, 47 (1935) 194–195.

[12] C.S. Smith, Piezoresistance effect in germanium and silicon, *Physical Review*, 94 (1954) 42–49.

[13] H.A. Nielsen, From Locomotives to Strain Gages, New York, Vantage Press, 1985.

[14] D.E. Stout, J.E. Sorensen, C. Kelleher, Write Right: Improving Written Communication Skills—Part Two, *Management Accounting Quarterly*, 16:4 (2015).

[15] B.S. Massey, I. Kavrak, A Miniature Pressure Transducer, *Journal of Scientific Instruments*, 43:8 (1966) 569–571.

[16] E. Stern, Solid–state sensors in process control, *Electrical Engineering*, 85:3 (1963) 332–335.

[17] H–P. Phan, D.V. Dao, K. Nakamura, S. Dimitrijev, N.T. Nguye, The Piezoresistive Effect of SiC for MEMS Sensors at High Temperatures: A Review, *Journal of Microelectromechanical Systems*, 24:6 (2015) 1663–1677.

[18] H. Tomlinson, On the increase in resistance to the passage of an electric current produced on wires by stretching, *Proceedings of the Royal Society of London*, 25 (1876) 451–453.

[19] V.J. Lumelsky, M.S. Shur, S. Wagner, Sensitive skin, *IEEE Sensors Journal*, 1:1 (2001) 41–51.

[20] L. Wang, Y. Li, A Review for Conductive Polymer Piezoresistive Composites and a Development of a Compliant Pressure Transducer, *IEEE Transactions on Instrumentation and Measurement*, 62: 2 (2013) 495–502.

[21] J.J. Carr, Sensors and Circuits, Englewood Cliffs: PTR Prentice Hall, 1993.

[22] M. Traite, W. Welkowitz, R. Downs, Intracardiac Catheter Tip Piezoresistive Pressure Gauge, *Review of Scientific Instruments*, 31:9 (1960) 987–991.

[23] A.C. Ruge, Gauge, Patent, US 2316975 A, 1943.

[24] T. Chiku and I. Igarashi, Needle–shaped pressure transducer, US Patent n. US3550583A, 1970

[25] H.W. Shirer, Blood Pressure Measuring Methods" *IRE Transactions on Bio–Medical Electronics*, 9:2, (1962) 116–125.

[26] P. Kantrowitz, Transducer Development for the Artificial Heart or Heart Assist Devices, *JAES*, 17:5 (1969) 539–549.

[27] R.H. Wyatt, A Study of Power Spectra Analysis of Normal Finger Tremors*" IEEE Transactions on Biomedical Engineering*, BME–15:1 (1968).

[28] J.S. Robinson, A.W. Wood, W. Thorp and C.T. Jones, A Possible Advance in Medical Manometry, *Brit. J. Anaesth.*, 41, (1969) 64–69.

[29] M. Maiwald, C. Werner, V. Zoellmer, M. Busse, INKtelligent printed strain gauges, *Sensors and Actuators A: Physical*, 162, (2010) 198–201.

[30] K. Bethe, The Scope of the Strain Gage Principle, *Proceedings. VLSI and Computer Peripherals COMPEURO 89*, Hamburg, Germany, 8–12 May, 1989.

[31] M.R. Lindeburg, Environmental Engineering Reference Manual, 2nd Edition, Belmont, CA, Professional Publications, Inc., 2003.

[32] L. Meyer, A unified rational analysis for gauge factor and cross–sensitivity of electric–resistance strain gauges, *The Journal of Strain Analysis for Engineering Design*, 2 (1967) 324–331.

[33] R.C. Weast, CRC Handbook of Chemistry and Physics, 62th Edition, CRC Press, Boca Raton, FL, 1981.

[34] S.E. Stanca, F. Hänschke, G. Zieger, J. Dellith, A. Dellith, A. Ihring, et al., Electro–architected porous platinum on metallic multijunction nanolayers to optimize their optical properties for infrared sensor application, *Nanotechnology*, 29 (2018) 1–12.

[35] R.L. Parker, A. Krinsky, Electrical Resistance Strain Characteristics of Thin Evaporated Metal Films, *Journal of Applied Physics*, 34 (1963) 2700–2708, 1963.

[36] W.P. Mason, Crystal Physics of interaction processes, Academic Press, NY, 1966.

[37] B.N. Streetman, Solid State Electronic Devices, Prentice–Hall, inc, Englewood cliffs, NJ, 2nd Edition, 1980.

[38] S.M. Sze, Physics of semiconductor devices, J. Wiley & Sons, lst ed., N.Y., 1969.

[39] W.G. Pfann, Isotropically piezoresistive semiconductor", *Journal of Applied Physics*, 33 (1962) 1618–1619.

[40] R.S. Okojie, A.A. Ned, A.D. Kurtz, W.N. Carr, Characterization of Highly Doped n– and p–Type 6H–SiC Piezoresistors, *IEEE Transactions on Electron Devices*, 45:4 (1998) 785–790.

[41] M. Kanaya, J. Takahashi, Y. Fujiwara, A. Moritani, Controlled sublimation growth of single crystalline 4H–SiC and 6H–SiC and identification of the polytypes by x–ray diffraction, *Applied Physics Letters*, 58 (1991) 56–58.

[42] D. Patranabis, Sensors and Transducers, 2nd ed., New Delhi, PHI Learning Pvt ltd., 2004.

[43] F. Bechstedt, P. Kackell, A. Zywietz, K. Karch, B. Adolph, K. Tenelsen, J. Furthmuller, Polytypism and properties of silicon carbide, *Physica Status Solidi (b)*, 202 (1997) 35–62.

[44] M. Aryafar, M. Hamedi, M.M. Ganjeh, A Novel Temperature Compensated Piezoresistive Pressure Sensor, *Measurement*, 63 (2015) 25–29.

[45] M.H. Bao, Micro Mechanical Transducers–Pressure Sensors, Accelerometers and Gyroscopes, Elsevier B.V., Amsterdam, The Netherlands, 2000.

[46] Q. Wang, J. Ding, W. Wang, Fabrication and temperature coefficient compensation technology of low cost high temperature pressure sensor, *Sensors and Actuators A: Physical*, 120 (2005) 468–473.

[47] Y. Liu, H. Wang, W. Zhao, H. Qin, X. Fang, Thermal–Performance Instability in Piezoresistive Sensors: Inducement and Improvement, *Sensors*, 16 (2016) 1–23.

[48] Z. Yao, T. Liang, P, Jia, Y, Hong, L. Qi, C. Lei, et al., Passive Resistor Temperature Compensation for a High–Temperature Piezoresistive Pressure Sensor, *Sensors*, 16:7 (2016).

[49] D. Hagner, Metal strain gages, in: Tactile sensors far robot and medicine, J. Webster Ed., New York, J. Wi1ey & Sons, 75–98, 1988.

[50] H.L. Trietley, Transducers in Mechanical and Electronic Design, New York: Marcel Dekker, Inc., 1986.

[51] L.E. Hollander, G.L. Vick, T.J. Diesel, The Piezoresistive Effect and its Applications, *Review of Scientific Instruments*. 31:3 (1960) 323–327.

[52] P.J. French, A.G.R. Evans, Piezoresistance in polysilicon and its applications to strain gauges, *Solid–State Electronics*, 32:1 (1989) 1–10.

[53] J.C. Doll, B.L. Pruitt, Piezoresistor Design and Applications, Springer, New York, NY, 2013.

[54] R. Taherian, Development of an Equation to Model Electrical Conductivity of Polymer–Based Carbon Nanocomposites, *Journal of Solid State Science and Technology*, 3:6 (2014) M26–M38, 2014.

[55] F. Lux, Models proposed to explain the electrical conductivity of mixtures made of conductive and insulating materials, *Journal of Materials Science*, 28 (1993) 285–301.

[56] L. Karásek, B. Meissner, S. Asai M. Sumita, Percolation Concept: Polymer–Filler Gel Formation, Electrical Conductivity and Dynamic Electrical Properties of Carbon–Black–Filled Rubbers, *Polymer Journal*, 28 (1996) 121–126.

[57] M.H. Al–Saleh, U. Sundarara, A review of vapor grown carbon nanofiber/polymer conductive composites, *Carbon*, 47, 2–22, 2009.

[58] R.A. Russell, An imaging force sensor for robotics applications, *National Conference on Robotics*, Melbourne, (1984) 123–127.

[59] W. Zhang, J. Suhr, N. Koratkar, Carbon nanotube/polycarbonate composites as multifunctional strain sensors, *J. Nanosci. Nanotechnol.*, 6 (2006) 960–964.

[60] G.T. Pham, Y.B. Park, Z. Liang, C. Zhang, B. Wang, Processing and modeling of conductive thermoplastic/carbon nanotube films for strain sensing", *Compos. Part B*, 39 (2008) 209–216.

[61] J.G: Rocha, A.J. Paleo, F.W.J. van Hattum, S. Lanceros–Mendez, Polypropylene–Carbon Nanofiber Composites as Strain–Gauge Sensor, *IEEE Sensors Journal*, 13:7 (2013) 2603–2609.

[62] K.J. Loh, J.P. Lynch, B.S. Shim, N.A. Kotov, Tailoring piezoresistive sensitivity of multilayer carbon nanotube composite strain sensors, *J. Intell. Mater. Syst. Struct*., 19 (2008) 747–764.

[63] T. Yasuoka, Y. Shimamura, A. Todoroki, Electrical resistance change under strain of CNF/flexible–epoxy composite, *Adv. Compos. Mater.*, 19 (2010) 123–138.

[64] N. Wang, X. Zhuoyan, P. Zhan, K. Dai, G. Zheng, C. Liu, et al., A tunable strain sensor based on a carbon nanotubes/electrospun polyamide 6 conductive nanofibrous network embedded into poly(vinyl alcohol) with self–diagnosis capabilities, *Journal of Materials Chemistry C*, 5 (2017) 4408–4418.

[65] V. Singh, D. Joung, L. Zhai, S. Das, S.I. Khondaker, S. Seal, Graphene based materials: past, present and future, *Prog. Mater. Sci.*, 56:8 (2011) 1178–1271.

[66] K.S. Novoselov, A.K. Geim, S.V. Morozov, D. Jiang, Y. Zhang, S.V. Dubonos, et al., Electric field effect in atomically thin carbon films, *Science*, 306 (2004) 666–669.

[67] A.K. Geim, K.S. Novoselov, The rise of graphene, *Nature Materials*, 6:3 (2004) 183–191.

[68] C. Lee, X. Wei, J.W. Kysar, J. Hone, Measurement of the elastic properties and intrinsic strength of monolayer graphene, *Science*, 321, (2008) 385–388.

[69] J.H. Chen, C. Jang, S. Xiao, M. Ishigami, M.S. Fuhrer, Intrinsic and extrinsic performance limits of graphene devices on SiO_2, *Nature Nanotechnology*, 3:4 (2008) 206–209.

[70] M.B. Coskun, L. Qiu, Md. S. Arefin, A. Neild, M. Yuce, D. Li, et al., Detecting Subtle Vibrations Using Graphene–Based Cellular Elastomers, *ACS Appl. Mater. Interfaces*, 9 (2017) 11345−11349.

[71] L. Qiu, J.Z. Liu, S.L.Y. Chang, Y. Wu, D. Li, Biomimetic superelastic graphene–based cellular monoliths, *Nature Communications*, 3 (2012) article number 1241.

[72] A. Rinaldi, A. Tamburrano, M. Fortunato, M.S. Sarto, A Flexible and Highly Sensitive Pressure Sensor Based on a PDMS Foam Coated with Graphene Nanoplatelets, *Sensors*, 16, (2016) 2148.

[73] X. Ye, Z. Yuan, H. Tai, W. Li, X. Dua, Y. Jianga, A wearable and highly sensitive strain sensor based on a polyethylenimine–rGO layered nanocomposite thin film, *Journal of Materials Chemistry C*, 117:1 (2005) 50–61.

[74] S. Iijima, Helical microtubules of graphitic carbon, *Nature*, 354 (1991) 56–58.

[75] S. Iijima, T. Ichihashi, Single–shell carbon nanotubes of 1–nm diameter, *Nature*, (1993) 363, 603–605.

[76] D. Bethune, C. Klang, M. De Vries, G. Gorman, R. Savoy, J. Vazquez, et al., Cobalt–catalysed growth of carbon nanotubes with single–atomic–layer walls, *Nature*, 363, (1993) 605–607.

[77] H. Chen, L. Miao Z. Su, Y. Song, M. Han, X. Chen, et al., Fingertip–inspired electronic skin based on triboelectric sliding sensing and porous piezoresistive pressure detection, *Nano Energy*, 40 (2017) 65–72.

[78] T. Yamada, Y. Hayamizu, Y. Yamamoto, Y. Yomogida, A.I. Najafabadi, D.N. Futaba, et al., A stretchable carbon nanotube strain sensor for human–motion detection, *Nature Nanotechnology*, 6 (2011) 296–301.

[79] D. Cho, J. Park, J. Kim, T. Kim, J. Kim, I. Park, et al., Three Dimensionally Continuous Conductive Nanostructure for Highly Sensitive and Stretchable Strain Sensor, *Applied Materials and Interfaces*, 9:20, (2017) 17369–17378.

[80] B. Philip, J.K. Abraham, A. Chandrasekhar, V.K Varadan, Carbon nanotube/PMMA composite thin films for gas–sensing applications, *Smart Materials and Structures*, 12:6 (2003) 935–939.

[81] J. Li, Y. Lu, M. Meyyappan, Nano Chemical Sensors with Polymer–Coated Carbon Nanotubes, *IEEE Sensors Journal*, 6:2 (2006) 1047–1051.

[82] S. Shang, Y. Yue, X. Wang, Piezoresistive strain sensing of carbon black /silicone composites above percolation threshold, *Review of Scientific Instruments*, 87:12 (2016) 123910–5.

[83] B. Wang, B.K. Lee, M.J. Kwak, D.W. Lee "Graphene/polydimethylsiloxane nanocomposite strain sensor, *Review of Scientific Instruments*, 84 (2013) 105005–4,.

[84] C. Lee, L. Jug, E. Meng, High strain biocompatible polydimethylsiloxane–based conductive graphene and multiwalled carbon nanotube nanocomposite strain sensors, *Applied Physics Letters*, 102 (2013) 183511–5.

[85] T. Gurunathan, C.R.K. Rao, R. Narayan, K.V.S.N. Raju, Polyurethane conductive blends and composites: Synthesis and applications perspective, *J. Mater Sci.*, 48:1 (2013) 67–80.

[86] P. Zhao, Y. Luo, J. Yang, D. He, L. Kong, P. Zheng, et al., Electrically conductive graphene–filled polymer composites with well organized three–dimensional microstructure, *Mater Lett.*, 121 (2014) 74–77.

[87] W. Xiaodong, H. Yangyang, Z. Xinxing, L. Canhui, Spirally Structured Conductive Composites for Highly Stretchable, Robust Conductors and Sensors, *ACS Applied Materials & Interfaces*, 9:27 (2017) 23007–23016.

[88] H. Hu, X Wang, J Wang, L Wan, F Liu, H Zheng, et al., Preparation and properties of graphene nanosheets–polystyrene nanocomposites via in situ emulsion polymerization, *Chemical Physics Letters*, 484 (2010) 247–253.

[89] F. Du, J.E. Fischer, K.I. Winey, Effect of nanotube alignment on percolation conductivity in carbon nanotube/polymer composites, *Physical Review B*, 72:12 (2005) 121404–4.

[90] N Jović, D Dudić, A Montone, Mv Antisari, M Mitrić, V Djoković, Temperature dependence of the electrical conductivity of epoxy/expanded graphite nanosheet composites, *Scripta Materialia*, 58, (2008) 846–849.

[91] W. Zheng, S.C. Wong, Electrical conductivity and dielectric properties of PMMA/expanded graphite composites, *Compos. Sci. Technol.*, 63 (2003) 225–235, 2003.

[92] H.B. Zhang, W.G. Zheng, Q. Yan, Y. Yang, J.W. Wang, Z.H. Lu, et al. "Electrically conductive polyethylene terephthalate/graphene nanocomposites prepared by melt compounding, *Polymer*, 51 (2010) 1191–1196.

[93] M. Ha, S. Lim, J. Park, D.S. Um, Y. Lee, H. Ko, Bioinspired interlocked and hierarchical design of ZnO nanowire arrays for static and dynamic pressure–sensitive electronic skins, Adv. Funct. Mater., 25 (2015) 2841–2849.

[94] L.W. Yap, S. Gong, Y. Tang, Y. Zhu, W. Cheng, Soft piezoresistive pressure sensing matrix from copper nanowires composite aerogel, *Science Bullettin*, 61:20 (2016) 1624–1630.

[95] C. Pang, G–Y Lee, T–I Kim, S.M, Kim, H.N. Kim, S–H Ahn, et al., A flexible and highly sensitive strain–gauge sensor using reversible interlocking of nanofibres, *Nature Materials*, 11 (2012) 795–801.

[96] H.P. Wang, D. Zhou, J. Cao, R. Lindeke, A Skin–Like Pressure Sensor Array Based on Silver Nanowires and Conductive Elastomer, *Conference on Smart Materials, Adaptive Structures and Intelligent Systems*, Snowbird, Utah, USA, 16–18 September, 2013.

[97] S. Gong, W. Schwalb, Y. Wang, Y. Chen, Y. Tang, J. Si, et al., A wearable and highly sensitive pressure sensor with ultrathin gold nanowires, *Nature Communications*, 5 (2014) article number 3132.

[98] Y. Zang, F. Zhang, C. Di, D. Zhu, Advances of flexible pressure sensors toward artificial intelligence and health care applications, *Materials Horizons*, 2 (2015) 140–156.

[99] C. Celle, A. Cabos, T. Fontecave, B. Laguitton, A. Beneyad, L. Guettaz, et al., Oxidation of copper nanowire based transparent electrodes in ambient conditions and their stabilization by encapsulation: Application to transparent film heaters, *Nanotechnology*, 29:8 (2018).

[100] C. Canali, D. Malvasi, B. Morten, M. Prudenziati, A. Taroni, Piezoresistive effects in thick–film resistors, *Journal of Applied Physics*, 51:6 (1980) 3282–3287.

[101] K.J. Puttlitz, P.A. Totta. "Area Array Interconnection Handbook, Springer Science + Business Media, New York, 2001.

[102] X. Chen, Z. Zhang, S. Liu, Thick film resistors on alumina substrate as sensing elements, *13th International Conference on Electronic Packaging Technology & High Density Packaging*, Guilin, China, 13–16 Aug., 2012.

[103] N.M. White, J.D. Turner, Thick–film Sensors: Past, Present and Future, *Meas. Sci. Technol.*, 8 (1997) 1–20.

[104] M. Prudentiziati, Handbook of Sensors and Actuators: Thick–films Sensors, 1, Ed. Elsevier, 1994,

[105] B.L. de Lima, A.N. Rodrigues da Silva, N. Morimoto, A Proposed Process to Fabricate Strain Gauge Directly Over the Sensor Substrate, *ECS Trans.*, 4:1 (2007) 123–130.

[106] D. Crescini, Load cell for dynamic force measurements: An example in Thick–Film Technology, *IEEE International Conference on Instrumentation and Measurement Technology*, Graz, Austria, 13–16 May, 2012.

[107] S. Guo, M. Miao, R. Fang, D. Hu, Y. Jin, A thick film accelerometer based on LTCC–technology, *13th International Conference on Electronic Packaging Technology & High Density Packaging*, Guilin, China, 13–16 Aug., 2012.

[108] S.A.A. Jabir and N.K. Gupta, Thick–Film Ceramic Strain Sensors for Structural Health Monitoring, *IEEE Transactions on Instrumentation and Measurement*, 60:11 (2011) 3669–3676.

[109] L.G. Occhipinti, E. Fontana, S. Smerzi, E. Spoto, M. Renna, A. Romano, et al., Flexible and conformable strain gauges for smart pressure sensors systems: Static and dynamic characterization, *15th IEEE International Conference on Nanotechnology*, Rome, Italy, 27–30 July, 2015.

[110] H. Tu, X. Chen, X. Feng, and Y. Xu, A post–CMOS compatible smart yarn technology based on SOI wafers, *Sensors and Actuators A: Physical*, 233 (2015) 397–404.

[111] N. Klejwa, N. Harjee, R. Kwon, S.M. Coulthard, B.L. Pruitt, Transparent SU–8 Three–Axis Micro Strain Gauge Force Sensing Pillar Arrays for Biological Applications, *International Conference on Solid–State Sensors, Actuators and Microsystems*, Lyon, France, 10–14 June, 2007.

[112] H.J. Xian, C.R. Cao, J.A. Shi, X.S. Zhu, Y.C. Hu, Y.F. Huang, et al., Flexible strain sensors with high performance based on metallic glass thin film, *Appl. Phys. Lett.*, 111 (2017) 121906–5.

[113] J. Engel, J. Chen, Z. Fan, C. Liu, Polymer micromachined multimodal tactile sensors, *Sensors and Actuators A: Physical*, 117:1 (2005) 50–61.

[114] J. Engel, J. Chen, C. Liu, Strain sensitivity enhancement of thin metal film strain gauges on polymer microscale structures, *Applied Physics Letters*, 89:22 (2006).

[115] J.A. Rogers, T. Someya, Y. Huang, Materials and Mechanics for Stretchable Electronics, *Science*, 327 (2010) 1603–1606.

[116] D.H. Kim and J.A. Rogers, Stretchable Electronics: Materials Strategies and Devices, *Advanced Materials*, 20 (2008) 4887–4892.

[117] M.I. Tiwana, S.J. Redmond, N.H. Lovell, A review of tactile sensing technologies with applications in biomedical engineering, *Sensors and Actuators A: Physical*, 179 (2012) 17–31.

[118] V. Bicchi and V. Kumar, Robotic grasping and contact: A review, *International Conference on Robotics and Automation (ICRA)*, 1, 348–353, San Francisco, USA, 24–28 April, 2000.

[119] F. Vidal–Verdú, O. Oballe–Peinado, J.A. Sánchez–Durán, J. Castellanos–Ramos, R. Navas–González, Three realizations and comparison of hardware for piezoresistive tactile sensors, *Sensors*, 11:3 (2011) 3249–3266.

[120] C. Lucarotti, C.M. Oddo, N Vitiello, M.C. Carrozza, Synthetic and Bio–Artificial Tactile Sensing: A Review, *Sensors*, 13:2 (2013) 1435–1466.

[121] Z. Liao, W. Liu, C. Zhang, Y. Zhang, X. Wang, X. Li, A tactile sensor translating texture and sliding motion information into electrical pulses, *Nanoscale*, 7:24 (2015) 10801–10806.

[122] A. Charalambides and S. Bergbreite, A novel all–elastomer MEMS tactile sensor for high dynamic range shear and normal force sensing, *J. Micromech. Microeng.*, 25 (2015) 095009–9.

[123] L.D. Harmon, Automated Tactile Sensing, *The International Journal of Robotics Research*, 1:2 (1982) 3–32.

[124] S. Stassi, V. Cauda, G. Canavese, C.F. Pirri, Flexible Tactile Sensing Based on Piezoresistive Composites: A Review, *Sensors*, 14:3 (2014) 5296–5332.

[125] A. Caiti, G. Canepa, D. De Rossi, F. Germagnoli, G. Magenes, T. Parisini, Towards the realization of an artificial tactile system: Fine–form discrimination by a tensorial tactile sensor array and neural inversion algorithms", *IEEE Transactions on Systems, Man, Cybernetics*, 25 (1995) 933–946.

[126] H.N. Norton, Handbook of Transducers, Englewood Cliffs: Prentice- Hall, Inc., 1989.

[127] K. Noda, K. Hoshino, K. Matsumoto; and I. Shimoyama, A shear stress sensor for tactile sensing with the piezoresistive cantilever standing in elastic material, *Sensors and Actuators A: Physical*, 127 (2006) 295–301.

[128] T. Takeshita, T. Kobayashi, R. Takei, T. Itoh, S. Takamatsu, Soft–rubber–packaged Pb(Zr,Ti)O3 MEMS touch sensors for human–machine interface applications, *Japanese Journal of Applied Physics*, 56 (2017) 04CC04–01–05.

[129] T. Okatani, H. Takahashi, K. Noda, T. Takahata, K. Matsumoto, I. Shimoyama, A Tactile Sensor Using Piezoresistive Beams for Detection of the Coefficient of Static Friction, *Sensors*, 16 (2016) 718.

[130] J. Zhou, W. Rong, L. Wang, P. Gao, L. Sun, A self–decoupling piezoresistive sensor for measuring microforce in horizontal and vertical directions, *Journal of Micromechanics and Microengineering*, 26:9 (2016) 095019–10.

[131] E. Laukhina, R. Pfattner, L.R. Ferreras, S. Galli, M. Mas–Torrent, N. Masciocchi, et al., Ultrasensitive Piezoresistive All–organic Flexible Thin Films, *Adv. Mater.*, 22:9 (2010) 977–981.

[132] C. Connolly, Switches and pressure sensors benefit from novel composite material, *Sensor Review*, 24:3 (2004) 261–264.

[133] R. Walker, Developments in dextrous hands for advanced robotic applications, *10th Int. Symp. Robot. App.*, Seville, Spain, 28 June– 1 July 2004.

[134] J. Engel, J. Chen and C. Liu, Development of polyimide flexible tactile sensor skin, *J. Micromech. Microeng.*, 13 (2003) 359–366.

[135] C. Stampfer, A. Jungen, R. Linderman, D. Obergfell, S. Roth, C. Hierold, Nano–Electromechanical Displacement Sensing Based on Single–Walled Carbon Nanotubes, *Nano Letters*, 6:7 (2006) 1449–1453.

[136] A.J. Brook, S.J. Bending, J. Pinto, A. Oral, D. Ritchie, H. Beere, et al., Micromachined III–V cantilevers for AFM–tracking scanning Hall probe microscopy, *J. Micromech. Microeng.*, 3 (2003) 124–128.

[137] Y. Penga, S. Itoa, Y. Shimizua, T. Azumaa, W. Gaoa, E. Niwa, A Cr–N thin film displacement sensor for precision positioning of a micro–stage, *Sensors and Actuators A: Physical*, 211 (2014) 89–97.

[138] J.A. Harley, T.W. Kenny, 1/f noise considerations for the design and process optimization of piezoresistive cantilevers, *Journal of Microelectromechanical Systems*, 9 (2000) 226–235.

[139] M. Rouff, Z. Lakhdari, M. Cotsaftis, S. Konieczka, Dynamical and thermal modelling of creep and relaxation for force and weight sensors, *Mechatronics*, 13 (2003) 77–84.

[140] R. Boynton ,Precise Measurement of Mass, *60th Annual Conference of the Society of Allied Weight Engineers*, Arlington, Texas, May 21–23, 2001.

[141] K.N. Bhat, Silicon Micromachined Pressure Sensors, *Journal of the Indian Institute of Science*, 87:1 (2007).

[142] R. Bogue, Recent developments in MEMS sensors: A review of applications, markets and technologies, *Sensor Review*, 33:4 (2013) 300–304.

[143] K.N. Bhat, M.M. Nayak, MEMS Pressure Sensors: An Overview of Challenges in Technology and Packaging, *Journal of ISSS*, 2:1 (2013) 39–71.

[144] S.S. Kumar, B.D. Pant, Design principles and considerations for the 'ideal' silicon piezoresistive pressure sensor: A focused review, *Microsystem Technology*, 20:7 (2014) 1213–1247.

[145] S.S. Kumar, B. D. Pant, Polysilicon thin film piezoresistive pressure microsensor: Design, fabrication and characterization, *Microsystem Technology*, 21:9 (2015) 1949–1958.

[146] G. Nakatani, MEMS Sensor", Us Patent US 8,387.459 B2, 2013.

[147] S. Coombs, Smart Skins: Information Processing by Lateral Line Flow Sensors", Autonomous Robots, 11 (2001) 255–261.

[148] B. Bathellier, F.G. Barth, J.T. Albert and J.A. Humphrey, Viscosity–mediated motion coupling between pairs of trichobothria on the leg of the spider Cupiennius Salei", *Journal of Comparative Physiology A*, 191:8 (2005) 733–746.

[149] S.J. Sterbing–D'Angelo, M. Chadha, K.L. Marshall, C.F. Moss, Functional role of airflow–sensing hairs on the bat wing", *Journal of Neurophysiology*, 117:2 (2017) 705–712.

[150] M. Le Masurier, P.G. Gillespie, Hair–Cell Mechanotransduction and Cochlear Amplification", *Neuron*, 48 (2005) 403–415.

[151] Z. Fan, J. Chen, J. Zou, D. Bullen, C. Liu and F. Delcomyn, Design and fabrication of artificial lateral line flow sensors", *Journal of Micromechanics and Microengineering*, 12 (2002) 655–661.

[152] N. Nguyen, D.L. Jones, Y.C. Yang and C. Liu, Flow vision for autonomous underwater vehicles via an artificial lateral line", *Journal on Advances in Signal Processing*, 2011 (2011) 1–11.

[153] S. Peleshanko, M.D. Julian, M. Ornatska, M.E. Mc Conney, M.C. LeMieux, N. Chen et al., Hydrogel–encapsulated microfabricated haircells mimicking fish cupula neuromast", *Advanced Materials*, 19 (2007) 2903–2909.

[154] Z. Shen, A.G.P. Kottapalli, V. Subramaniam, M. Asadnia, J. Miao, M. Triantafyllou, Biomimetic Flow Sensors for Biomedical Flow Sensing in Intravenous Tubes", *IEEE Sensors Conference*, Orlando, Florida, USA, 30 October–3 November 2016.

[155] Y.–H. Wang, C.–Y. Lee and C.–M. Chiang, A MEMS–based Air Flow Sensor with a Free–standing Microcantiveler Structure", *Sensors*, 7 (2007) 2389–2401.

[156] S. Zhang, L. Lou, C. Lee. "Piezoresistive silicon nanowire based nanoelectromechanical system cantilever air flow sensor", *Applied Physics Letters*, 100:2 (2012) 023111–023113.

[157] A.R. Aiyar, C. Song, S.–H. Kim, M.G. Allen, An all–polymer airflow sensor using a piezoresistive composite elastomer", *Smart Materials and Structures*, 18 (2009) 115003–9.

[158] C. Jacq, B. Lüthi, Th. Maeder, O. Lambercy, R. Gassert, P. Ryser. "Thick–film multi–DOF force/torque sensor for wrist rehabilitation", *Sensors and Actuators A: Physical*, 168 (2010) 361–366.

[159] J. Caroline, T. Maeder, S. Emery, M. Simoncini, E. Meurville, P. Ryser. "Investigation of Polymer Thick–Film Piezoresistors for Medical Wrist Rehabilitation and Artificial Knee Load Sensors", *Procedia Engineering*, 87 (2014) 1194–1197.

[160] H. Khan, M. D'Imperio, F. Cannella, D.G. Caldwell, A. Cuschieri and C. Semini. "Towards Scalable Strain Gauge–Based Joint Torque Sensors", *Sensors*, 17 (2017) 1905, 1–17.

[161] L.M. Roylance, J.B. Angell. "A batch–fabricated silicon accelerometer, *IEEE Transaction on Electron Devices*, 26:12 (1979) 1911–1917.

[162] J. Fraden. Handbook of Modern Sensors; Physics, Design, Applications, Fourth Edition, Springer Press, 2010.

[163] P. Dong, X. Li, Y. Wang, S. Feng. "An Axial–beam Piezoresistive Accelerometer for Highperformance Crash Detection of Automotive Industry", *IEEE Sensors Conference*, Daegu, South Korea, 22–25 October 2016.

[164] S. Chitta, P. Vemaza, R. Geykhman. and D.D. Lee. "Proprioceptive localization for a quadrupedal robot on known terrain", *IEEE International Conference on Robotics and Automation*, Roma, Italy, 10–14 April, 2007.

[165] P.H. Mansur, L.K. Cury, A.O. Andrade, A.A. Pereira, G.A. Miotto, A.B. Soares, E.L. Naves. "A review on techniques for tremor recording and quantification", *Critical Reviews in Biomedical Engineering*, 35:5 (2007) 343–362.

[166] S. Biswas, A.K. Gogoi. "Design of a Piezoresistive Microaccelerometer with High Sensitivity for Medical Diagnostic", In: A. Konkani, R. Bera, S. Paul (eds), Advances in Systems, Control and Automation. Lecture Notes in Electrical Engineering, 442, Springer, Singapore, 2018.

[167] S. Franco, Design with Operational Amplifier and Analog Integrated Circuits, India: TMH 91–97, 2002.

[168] S. Gift and B. Maundy, Strain Gauge Amplifier Circuits, *IEEE Transactions on Instrumentation and Measurement*, 62:4 (2013) 693–700.

[169] D.J. Yonce, P.P. Bey, T.L. Fare, A DC Autonulling Bridge for Real–Time Resistance Measurement, *IEEE Transactions on Circuits and Systems I: Fundamental Theory and Applications*, 47:3 (2000) 273–278.

[170] E. Farshidi, A Low–Voltage Current–Mode Wheatstone Bridge using CMOS Transistors*;" International Journal of Electrical and Electronics Engineering*, 5:1 (2011) 38–42.

[171] S. Gift and B. Maundy, New configuration for the measurement of small resistance changes", *IEEE Trans. Circuits and Systems–II: Express Brief*, 53:3 (2006) 178–182.

[172] I.F. Akyildiz, W. Su, Y. Sankarasubramaniam, E. Cayirci, A survey on sensor networks, *IEEE Communications Magazine*, 40:8 (2002), 102–114.

[173] I. Clausen, T. Glott, Development of Clinically Relevant Implantable Pressure Sensors: Perspectives and Challenges, *Sensors* 14 (2014) 17686–17702.

[174] K. Arshak, G. Lyons, L. Cavanagh, S. Clifford, Front- end signal conditioning used for resistance-based sensors in electronic nose systems: a review, *Sensor Review*, 23:3 (2003) 230–241

[175] A. Loui, T.V. Ratto, T.S. Wilson, S.K. McCall, E.V. Mukerjee, A.H. Love, B.R. Hart, Chemical vapor discrimination using a compact and low–power array of piezoresistive microcantilevers, *Analyst*, 133:5 (2008) 608–615.

[176] J.D. Adams, G. Parrott, C. Bauer, T. Sant, L. Manning, M. Jones, B. Rogers, Nanowatt chemical vapor detection with a self–sensing, piezoelectric microcantilever array, *Applied Physics Letters*, 83:16 (2003) 3428–3430.

[177] M. Crego- Calama, S. Brongersma, D. Karabacak, M. Van Bavel, A low- power integrated electronic nose system, *Sensor Review*, 32:1 (2012) 72–76

[178] P.D. Harris, W.M. Arnold, M.K. Andrews, A.C. Partridge, Resistance characteristics of conducting polymer films used in gas sensors, *Sensors and Actuators B: Chemical*, 42 (1997) 177–184.

[179] M.A. Cullinan, R.M. Panas, C.M. Di Biasio, M.L. Culpepper, Scaling electromechanical sensors down to the nanoscale, *Sensors and Actuators A: Physical*, 187 (2012) 162–173.

[180] Falconi, C. Di Natale, A. D'Amico, M. Faccio, Electronic interface for the accurate read–out of resistive sensors in low voltage–low power integrated systems, *Sensors and Actuators A: Physical*, 117 (2005) 121–126.

[181] A. Thanachayanont, S. Sangtong,Low- Voltage Current- Sensing CMOS Interface Circuit for Piezo- Resistive Pressure Sensor, *ETRI Journal*, 29:1 (2007) 70–78.

[182] J.F. Creemer, F. Fruett, G.C.M. Meijer, P.J. French, The piezojunction effect in silicon sensors and circuits and its relation to piezoresistance,'' IEEE Sensors Journal, 1 (2001) 98–108.

[183] M. Doelle, C. Peters, P. Ruther, O. Paul, Piezo–FET Stress–Sensor Arrays for Wire–Bonding Characterization, Journal of Microelectromechanical Systems, 15:1 (2006) 120–130.

[184] R.G. Beck, M.A. Eriksson, M.A. Topinka, R.M. Westervelt, K.D. Maranowski, A.C. Gossard, GaAs/AlGaAs self-sensing cantilevers for low temperature scanning probe microscopy, *Applied Physics Letters* 73:8 (1998) 1149–1151.

[185] E.M. Boujamaa, B. Alandry, S. Hacine, L. Latorre, F. Mailly, P. Nouet, A Low Power Interface Circuit for Resistive Sensors with Digital Offset Compensation, *IEEE International Symposium on Circuits and Systems*, (2010).

[186] N. Dumas, S. Hacine, F. Mailly, L. Latorre, P. Nouet, A tracking converter for resistive sensors based on a feedback active bridge, IEEE 9th International on New Circuits and Systems Conference, (2011) 458–461.

[187] V. Garcia, F. Fruett, A mechanical–stress sensitive differential amplifier, *Sensors and Actuators A: Physical*, 132 (2006) 8–13.

[188] G. de Oliveira Coraucci, F. Fruett "Study, design, microfabrication and characterization of a new CMOS compatible multi–terminal pressure sensor with enhanced sensitivity, *Sensors and Actuators A: Physical*, 165 (2011) 43–53.

[189] P. Gonzalez, M. Rakowski, D. San Segundo, S. Severi, K. de Meyer, A. Witvrouw, CMOS–Integrated Poly–SiGe Piezoresistive Pressure Sensor, *IEEE Electron Device Letters*, 33:8 (2012) 1204–1206.

[190] A. Donida and D. Barrettino, A Low–Power Interface Circuit for Piezoresistive Transducers, *IEEE International Conference on Instrumentation and Measurement Technology*, Pisa, Italy, 11–14 May, 2015.

[191] Y. Deimerly, Towards ultra–compact inertial platforms based on piezoresistive nanogauges: focus on co–integration issues, Ph.D: dissertation, Electronics Université Paris–Est, 2013.

[192] N.A. Gilda, S. Nag, S. Patil, M.S. Baghini, D.K. Sharma, V.R. Rao, Current Excitation Method for ΔR Measurement in Piezo–Resistive Sensors with a 0.3–ppm Resolution, *IEEE Transactions on Instrumentation and Measurement*, 61:3 (2012) 767–774.

[193] A.S. Sedra and G. W. Roberts, Current conveyor theory and practice, In: Analogue IC Design: The Current Mode Approach, C. Toumazou, F. J. Lidgey, D. G. Haigh, Eds. London, U.K.: Peter Peregrinus, Ltd., 1990.

[194] J. Samitier, M. Puig–Vidal, S.A. Bota, C. Rubio, S.K. Siskos, T. Laopoulos, A Current–Mode Interface Circuit for a Piezoresistive Pressure Sensor, *IEEE Transactions on Instrumentation and Measurement*, 47:3 (1998).

[195] G. Ferri, V. Stornelli, M. Fragnoli, An integrated improved CCII topology for resistive sensor application, *Analog Integr. Circ. Sig. Process.*, 48 (2006) 247–250.

[196] A. De Marcellis, G. Ferri, P. Mantenuto, Analog Wheatstone bridge–based automatic interface for grounded and floating wide–range resistive sensors, *Sensors and Actuators B: Chemical*, 187 (2013) 371–378.

[197] A.J. Lopez–Martin, M. Zuza, A. Carlosena, Analysis of a NIC as a temperature compensator for bridge sensors, *IEEE Transactions on Instrumentation and Measurement*, 52:4 (2003) 1068–1072.

[198] A.J. Lopez–Martin, A. Carlosena, Low–Cost Analog Interface Circuit for Resistive Bridge Sensors , *13th International Symposium on Communications and Information Technologies*, Surat Thani, Thailand, 4–6 Sept., 2013.

[199] S. Yang, L. Wang, X. Tian, Z. Xu, W. Wang, X. Bai, et al., The Piezotronic Effect of Zinc Oxide Nanowires Studied by in–situ TEM, *Adv. Mater.*, 24 (2012) 4676–4682.

[200] T. Toriyama, D. Funai, S. Sugiyama, Piezoresistance measurement on single crystal silicon nanowires, Journal of Applied Physics, 93:1 (2003) 561–565.

[201] D.V. Dao, T. Toriyama, S. Sugiyama, Noise and Frequency Analyses of a Miniaturized 3–DOF Accelerometer Utilizing Silicon Nanowire Piezoresistors, *IEEE Sensors Conference*, Vienna, Austria, 24–27 Oct., 2004.

[202] T. Toriyama, Y. Tanimoto, S. Sugiyama. Single crystal silicon nano–wire piezoresistors for mechanical sensors, *Journal of Microelectromechanical Systems*, 11:5 (2002) 605–611.

[203] S. Vetrivel, R. Mathew, R. Sankar, Design and optimization of a doubly clamped piezoresistive acceleration sensor with an integrated silicon nanowire piezoresistor, *Microsystem Technologies*, 23:8 (2017) 3525–3536.

[204] M. Messina, J. Njuguna, V. Dariol, C. Pace, G. Angeletti, Design and Simulation of a Novel Biomechanic Piezoresistive Sensor with Silicon Nanowires, *IEEE/ASME Transactions on Mechatronics*, 18:3 (2013) 1201–1210.

[205] K. Matsudaira, T–V Nguyen, K.H. Shoji, T. Tsukagoshi, T. Takahata, I. Shimoyama, MEMS piezoresistive cantilever for the direct measurement of cardiomyocyte contractile force, *Journal of Micromechanics and Microengineering*, 27:10 (2017).

[206] S. Dellea, A. Longoni, G. Langfelder, A. Nikas, O. Leman, J. Hauer, et al., A comprehensive study of NEMS–based piezoresistive gyroscopes for vestibular implant systems, *IEEE International Symposium on Inertial Sensors and Systems*, Kauai, HI, USA, 27–30 March 2017.

[207] Y.S. Rim, S.–H. Bae, H. Chen, N. De Marco, Y. Yang. "Recent Progress in Materials and Devices toward Printable and Flexible Sensors, *Adv. Mater.*, 28 (2016) 4415–4440.

[208] B. Kim and E. Meng, Review of polymer MEMS micromachining, *Journal of Micromechanics and Microengineering*, 26:1 (2016) 013001–21.

[209] X. Li, R. Zhang, W. Yu, K. Wang, J. Wei, D. Wu, et al., Stretchable and highly sensitive graphene–on–polymer strain sensors, *Scientific Reports*, 2 (2012).

[210] Y. Ma, N. Liu, L. Li, X. Hu, Z. Zou, J. Wang, et al., A highly flexible and sensitive piezoresistive sensor based on MXene with greatly changed interlayer distances, *Nature Communications*, 8 (2017) article number 1207.

[211] D–H. Kim, N. Lu, R. Ma, Y–S. Kim, R–H. Kim, S. Wang, et al., Epidermal Electronics, *Science*, 333:6044 (2011) 838–843.

[212] W.R. Loewenstein and R. Skalak, Mechanical transmission in a Pacinian corpuscle. An analysis and a theory, *The Journal of Physiology*, 182:2 (1966) 346–378.

[213] L.A. Jones A.M. Smith, Tactile sensory system: Encoding from the periphery to the cortex, *Wiley Interdisciplinary Reviews: Systems Biology and Medicine*, 6:3 (2014) 279–287.

[214] A.P. Chandrakasan, N. Verma, D.C. Daly, Ultralow-Power Electronics for Biomedical Applications, *Annual Review of Biomedical Engineering*, 10 (2008) 247–274.

Antonino S. Fiorillo graduated in Electronic Engineering in 1984 and earned a Ph.D. in Electronic Devices and Technologies in 1988, both at the University of Pisa, Italy. From 1984 to 1991 he was a research scientist at the "Centro E. Piaggio" School of Engineering, at the same university, where he was involved in the development of proximity and tactile sensors based on ferroelectric polymer technology for robotic applications. He had been an assistant professor at the University of Salerno and the University of Sannio, from 1991 to 2003, when he was awarded the position of associate professor in electronics and sensors at the University of Magna Græcia in Catanzaro, Italy, where he is presently working. He was visiting scientist from 1987 to 1997, and then visiting professor from 1997 to 2002 at the "Center of Sensor Technologies" of the University of Pennsylvania, PA. His primary research interests are in the area of discrete and silicon integrated sensors based on ferroelectric and conducting polymers for application in the fields of robotics and medicine, besides electrical brain stimulation, and the interfacing of electronic and biological systems with nanoporous materials on silicon.

Costantino Davide Critello completed his Bachelor's and Master's degrees in Biomedical Engineering at the University Magna Graecia of Catanzaro (Italy) in 2007 and 2011, respectively. He also received from the same University a 2nd level postgraduate specialization in Biomedical Electronics in 2013, and his Doctoral degree in Biomedical Engineering in 2016.

He is currently working as post-doctoral researcher in the Department of Health Sciences at the University Magna Graecia of Catanzaro (Italy). His main research interests focus on piezoelectric sensors, ultrasound, cavitation generation, and development and characterization of soft materials.

Salvatore A. Pullano received the B.S. and M.S. degrees in electronic engineering from the University of Calabria, Italy, and the Ph.D. in Biomedical Engineering and Computer Science from the University Magna Græcia of Catanzaro, Italy. Currently, he is a Post-Doctoral Fellow in the Department of Health Sciences at the University Magna Græcia of Catanzaro, Italy and Adjunct Assistant Professor at the University of Tennessee-Knoxville. His research interests include the design of pyroelectric and piezoelectric sensors, electronic systems and nanoporous materials for biomedical applications.

Figure Captions

Fig. 1. Literature involving the use of the piezoresistive effect from 1960-2018. Source: Scopus.

Fig. 2. a) Piezoresistive bar to which traction is applied. b) Cross-section of a planar strain gauge to which an electrical potential *V* is applied along the width *W*, while traction is applied along the length *l*, orthogonal to the page (transverse piezoresistive effect).

Fig. 3. a) Energy plot of free particle (dotted line) compared to that of a particle (continuous line) which moves in an ordered structure of potential wells; when the energy *E* increases the two curves tend to partially overlap in the allowed bands (not shown in Fig.). b) Second derivative of energy versus the wave number.

Fig. 4. Minimum energy surfaces for a) germanium, b) gallium arsenide, and c) silicon in unstrained state (solid lines) and by applying external stress (dashed lines). The mobility μ_T, and μ_L represent the components, perpendicular and longitudinal, respect to the principal axis.

Fig. 5. Conduction band and valence band in silicon along [111] and [100] *k*-directions [38].

Fig. 6. a) Conductive particles dispersed in an insulating matrix. b) The origin of an electrical conduction path at the percolation threshold b).

Fig. 7. Conductive rubber tactile sensor.

Fig. 8. Various strain gauge configurations.

Fig. 9. Two different configuration of force/displacement transducer.

Fig. 10. Etching process steps for Si-cantilever production (only one electrode is shown).

Fig. 11. Cruciform pressure sensor etched on a silicon membrane (not shown).

Fig. 12. Indirect flow measurement.

Fig. 13. Torque sensor in which two strain gauges along a diagonal experience a traction, while the other two (along the other diagonal) experience a compression.

Fig. 14. Acceleration sensor.

Fig. 15. Wheatstone Bridge connected to a differential dc amplifier.

Fig. 16. Instrumentation or differential buffer amplifier.

Fig. 17. Half Bridge connected to a current-to-voltage converter.

Fig. 18. Double current-to-voltage converter [3].

Fig. 19. On-silicon integrated Wheatstone bridge cascaded with a CMOS differential amplifier.

Fig. 20. Timeline of the main steps in the development of piezoresistive sensor technology.

Figures

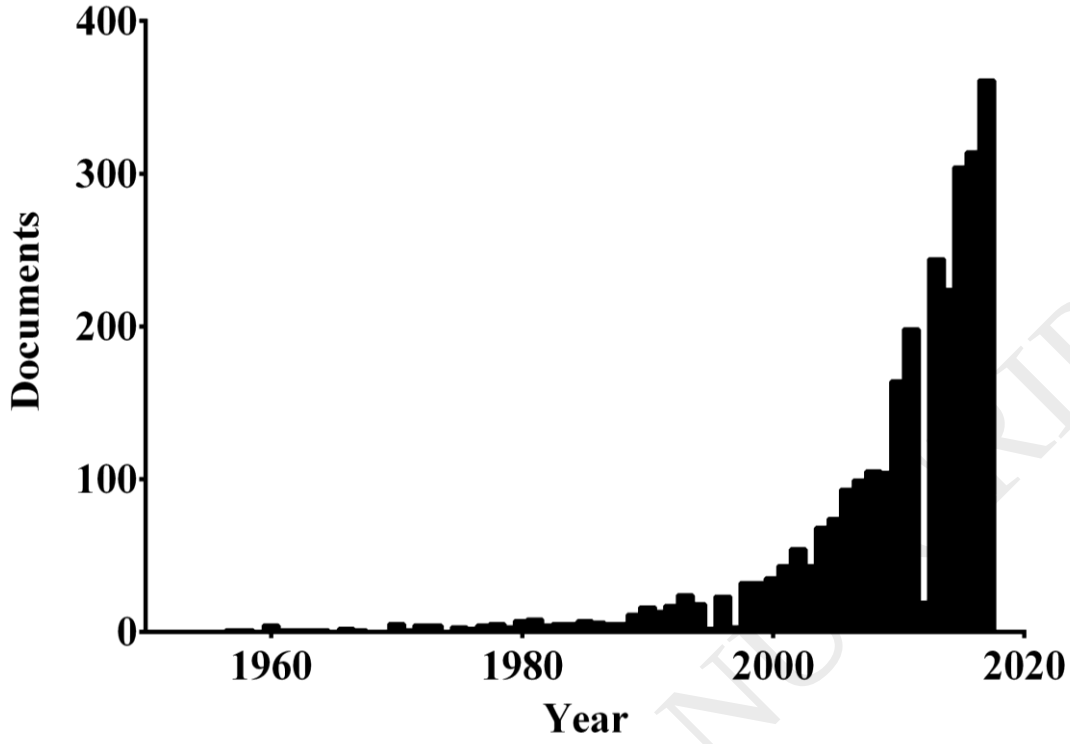

Figure 1

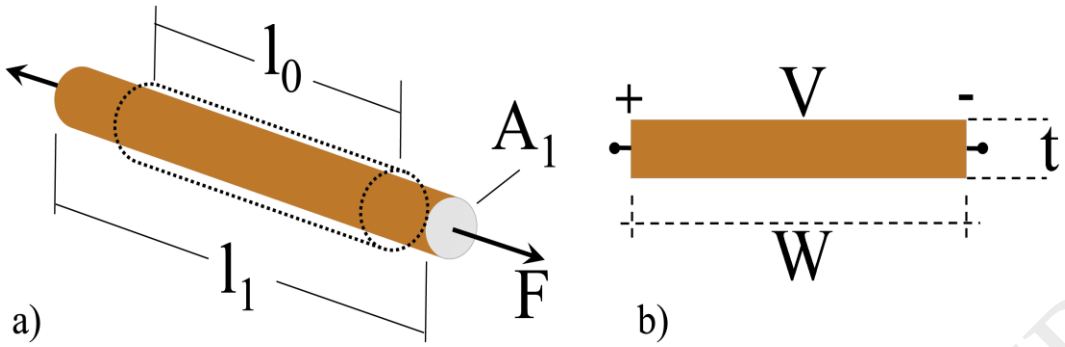

Figure 2

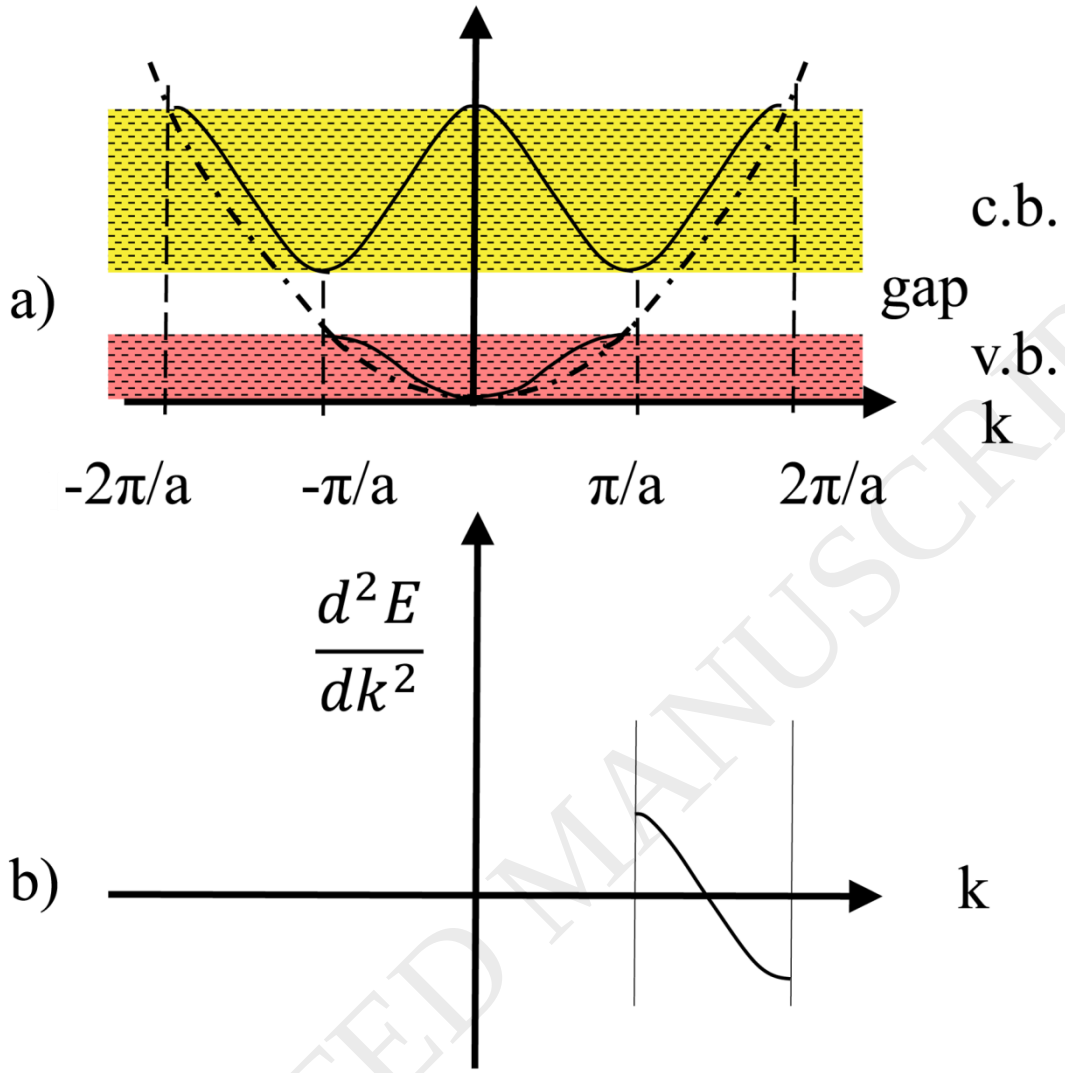

Figure 3

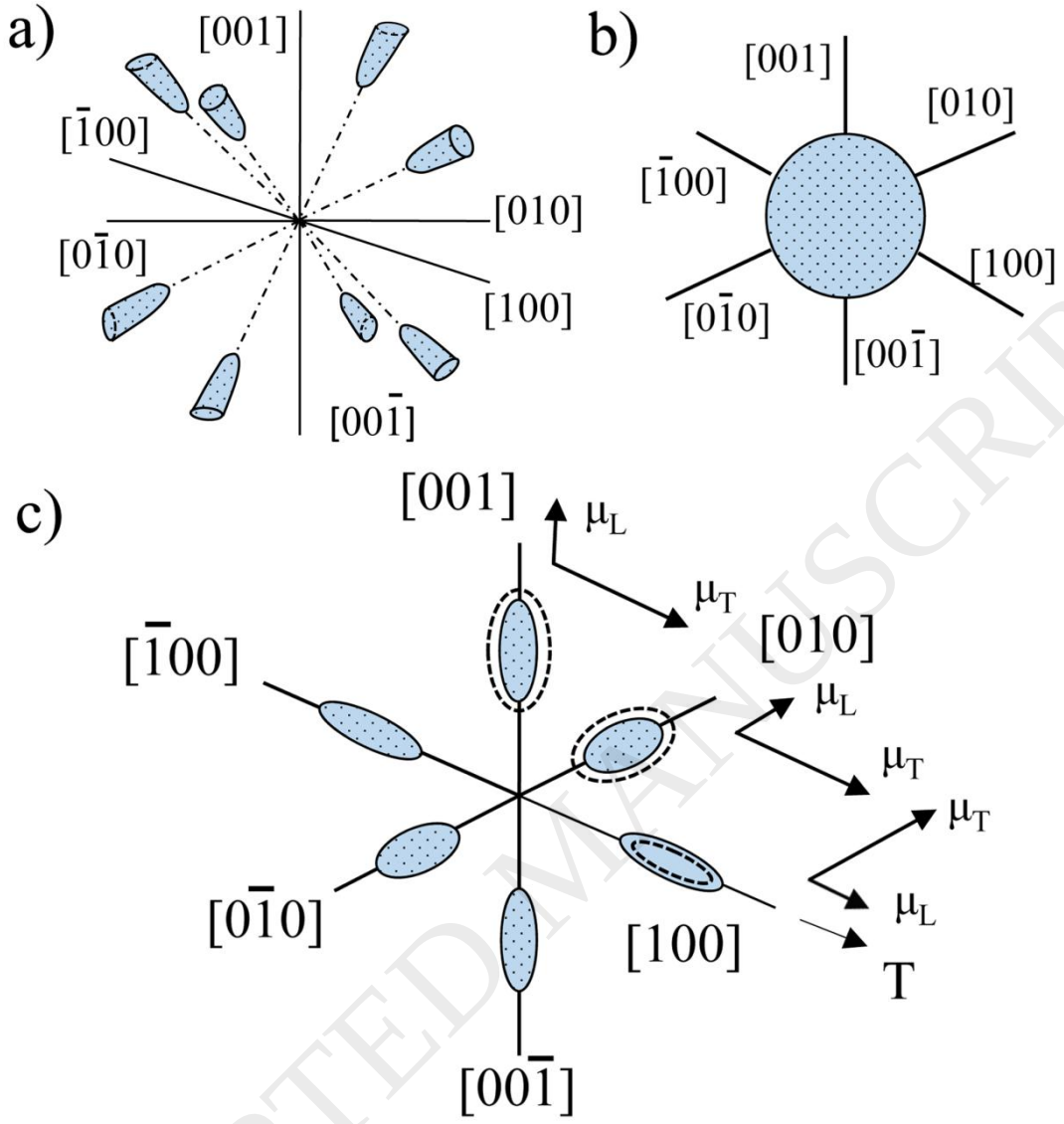

Figure 4

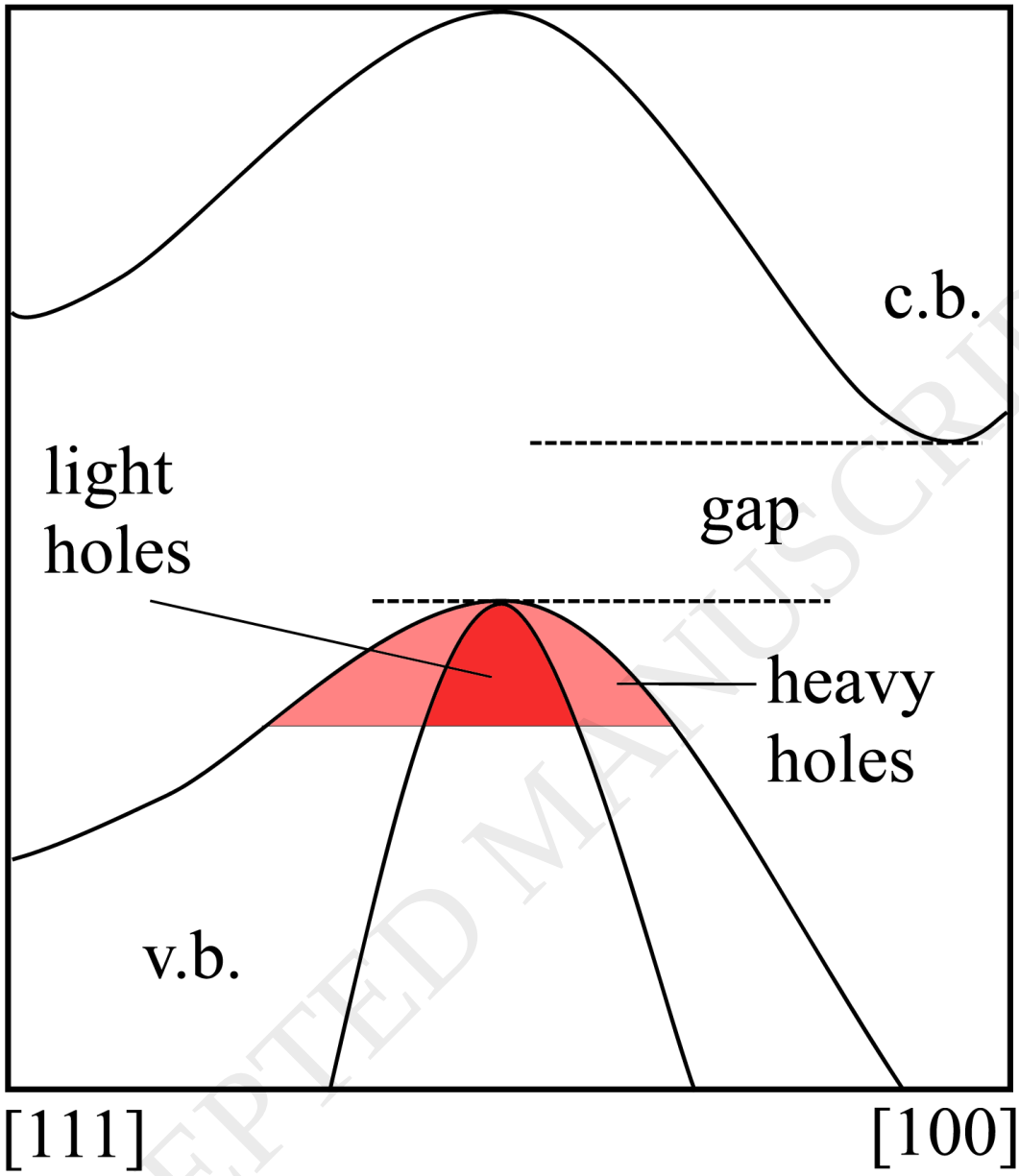

Figure 5

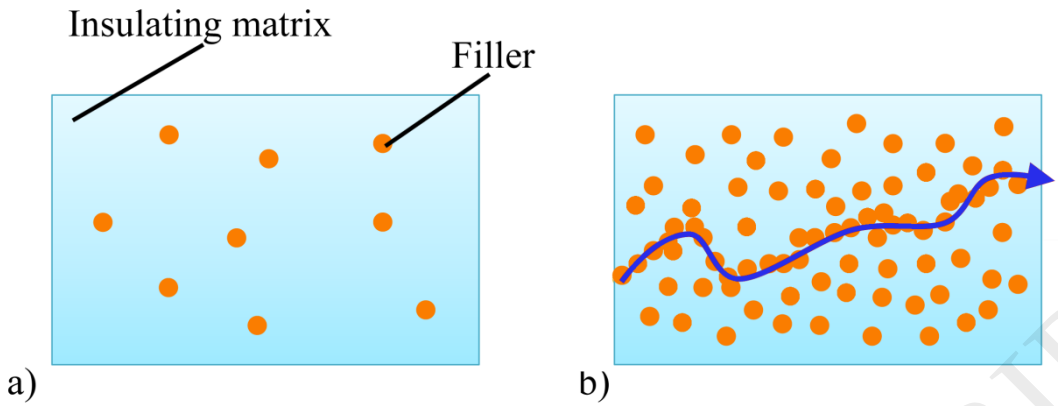

Figure 6

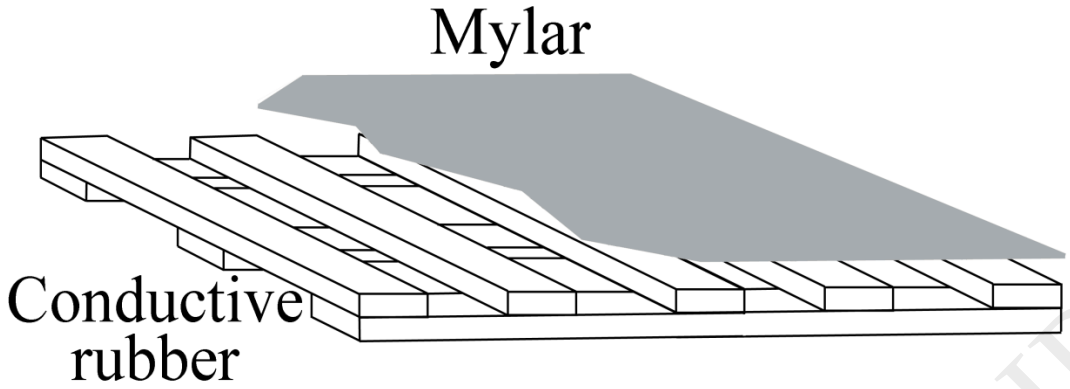

Figure 7

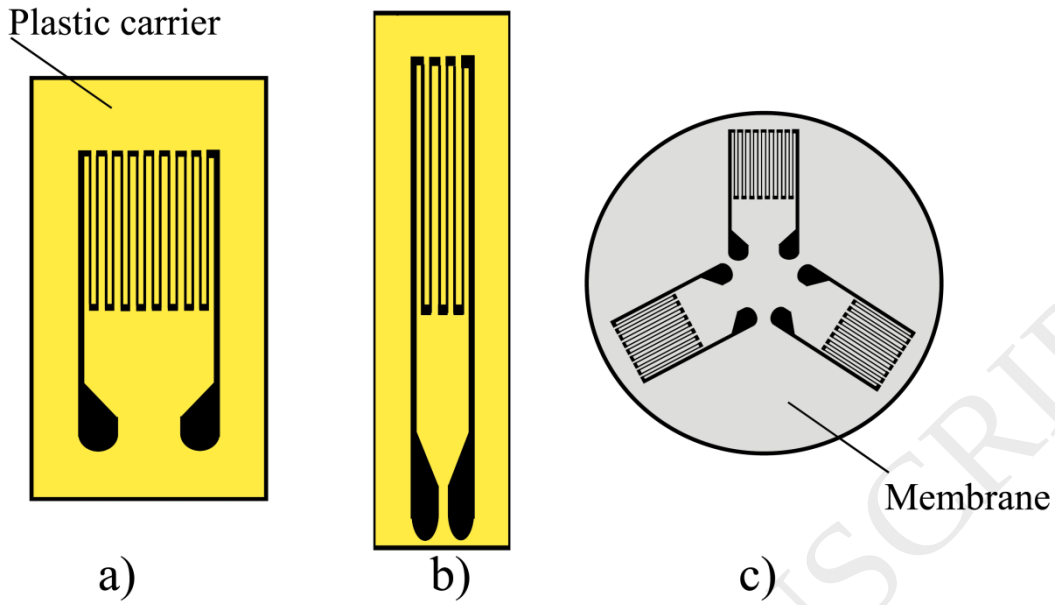

Figure 8

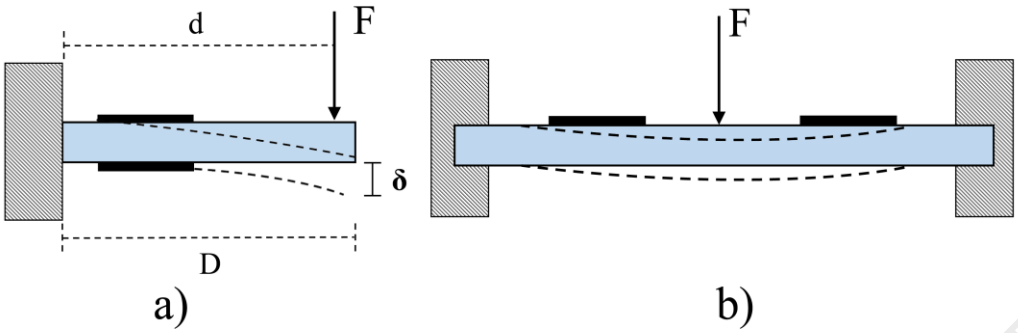

Figure 9

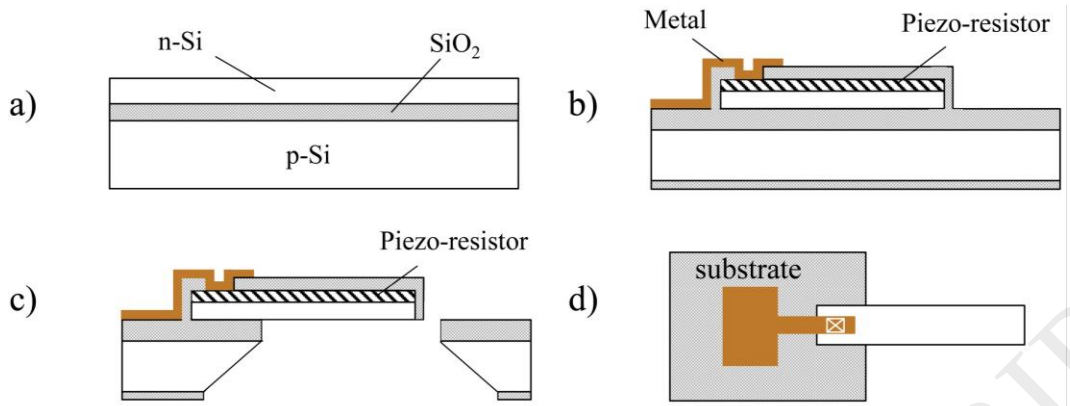

Figure 10

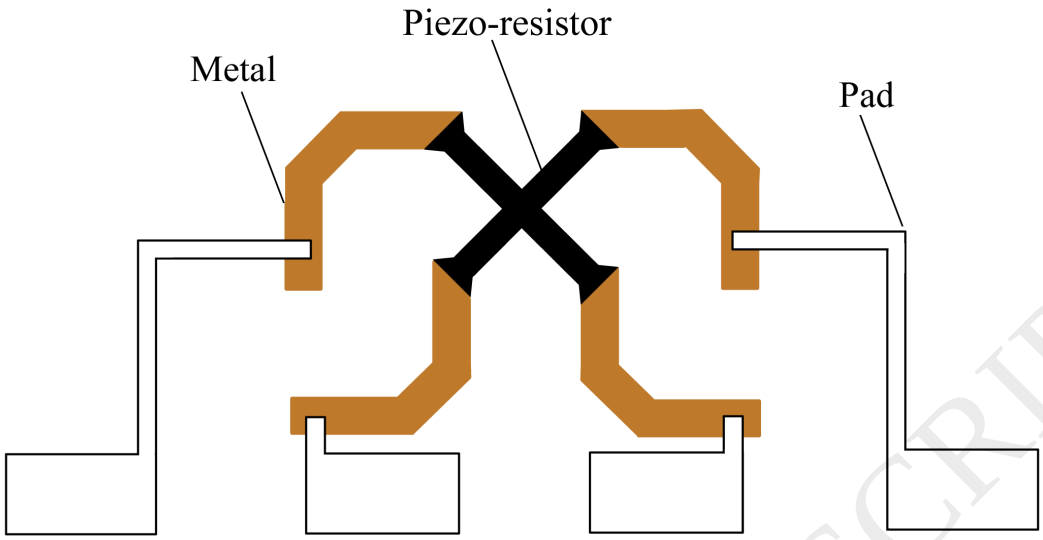

Figure 11

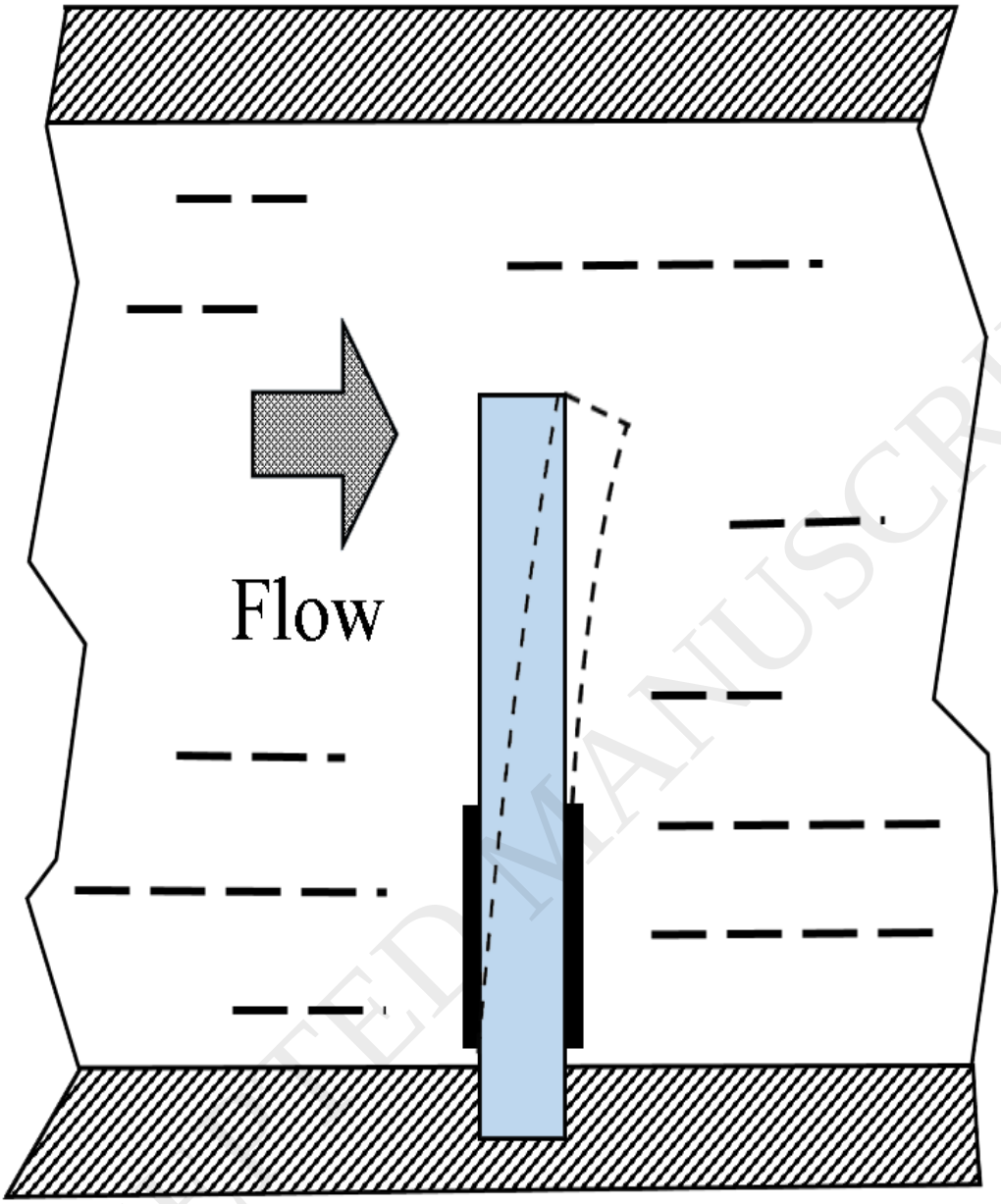

Figure 12

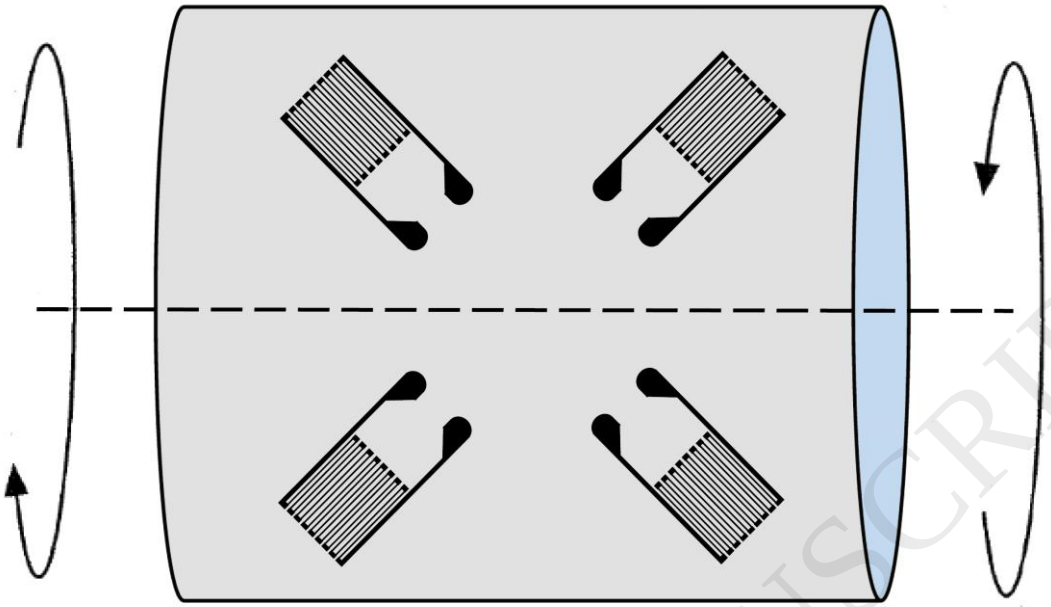

Figure 13

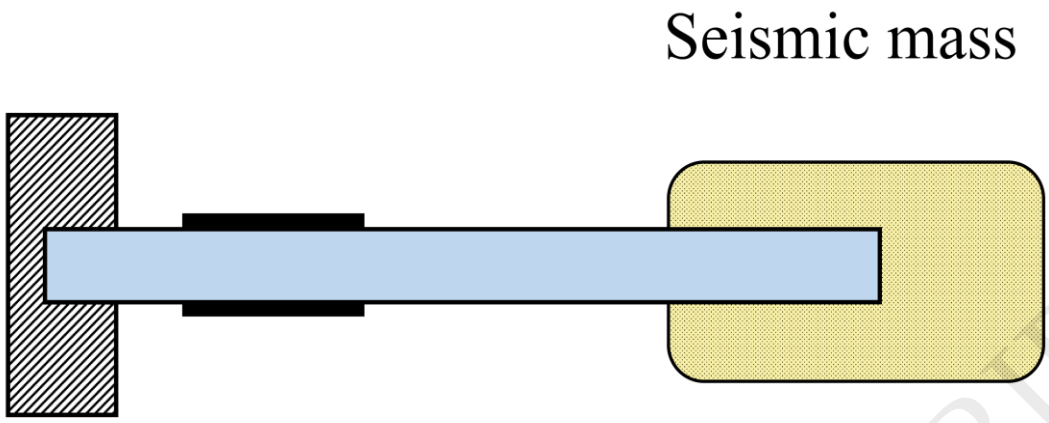

Figure 14

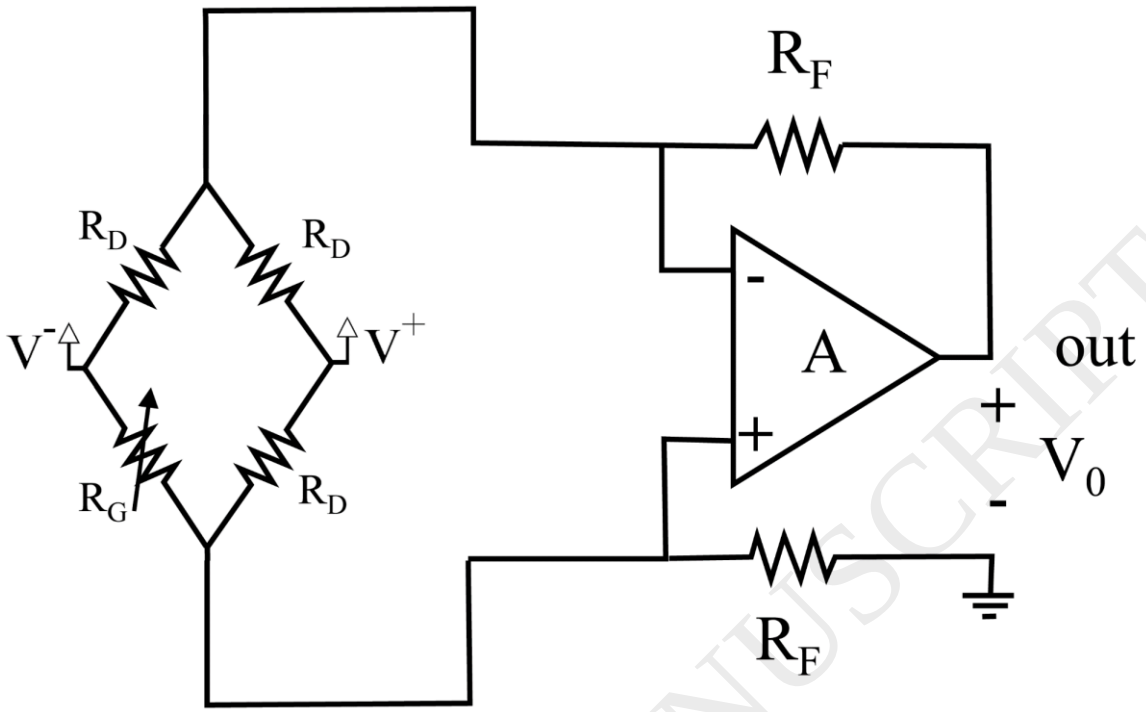

Figure 15

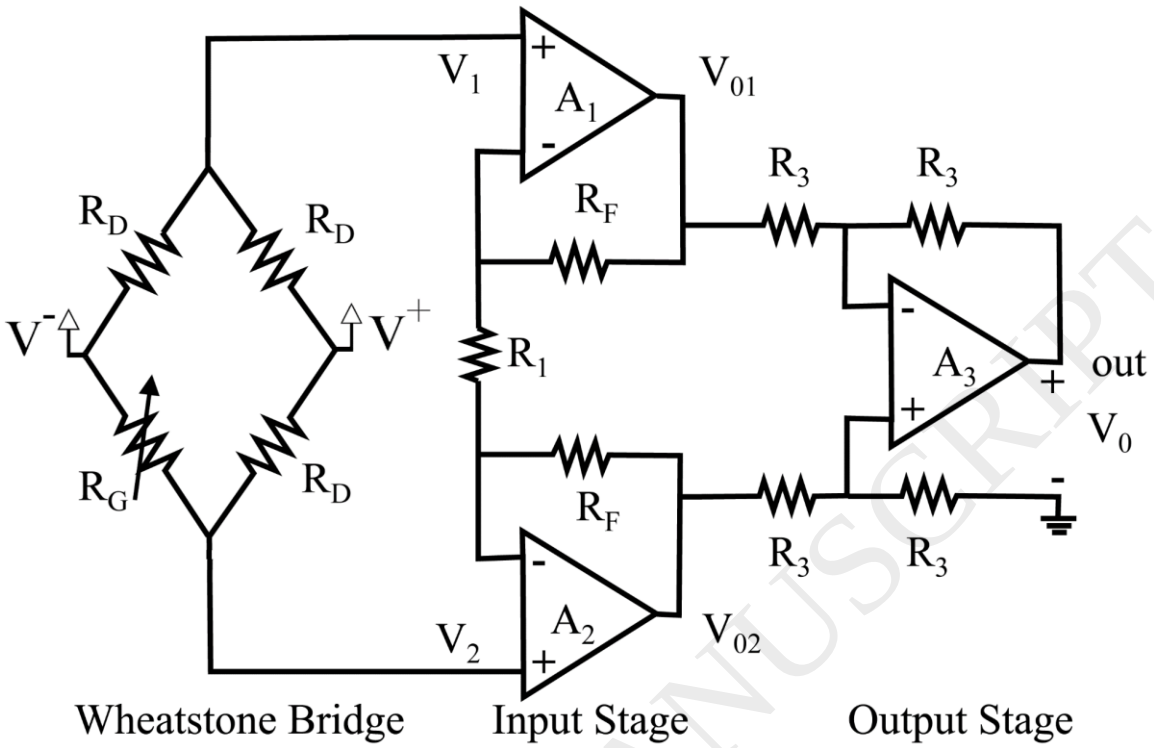

Figure 16

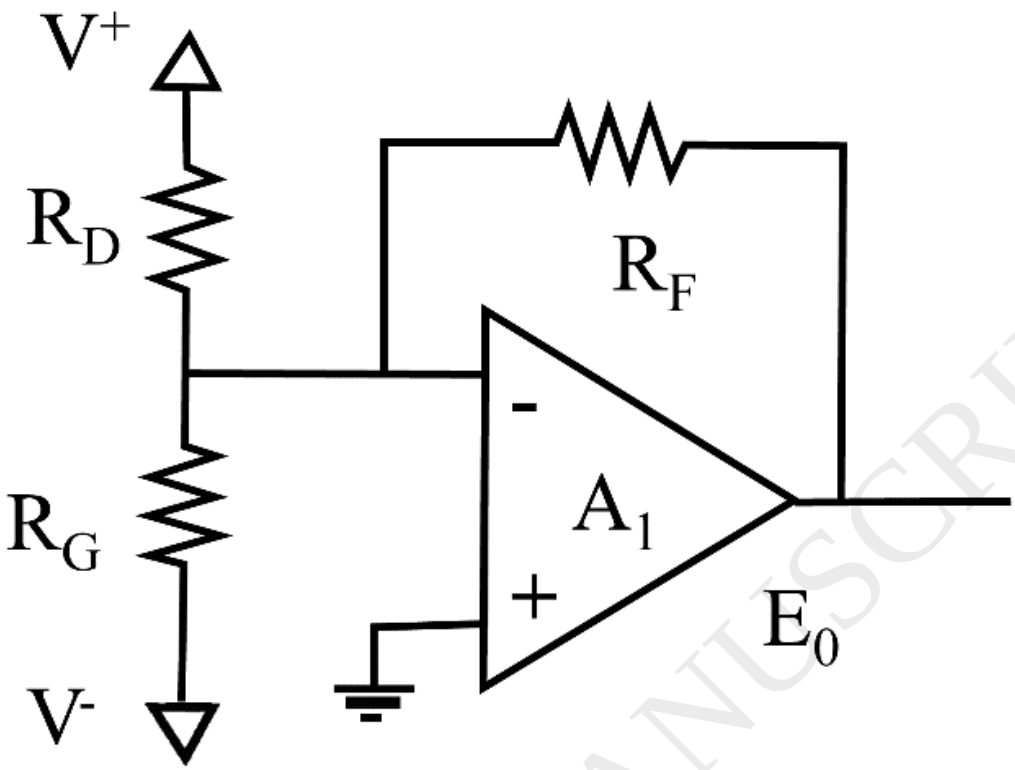

Figure 17

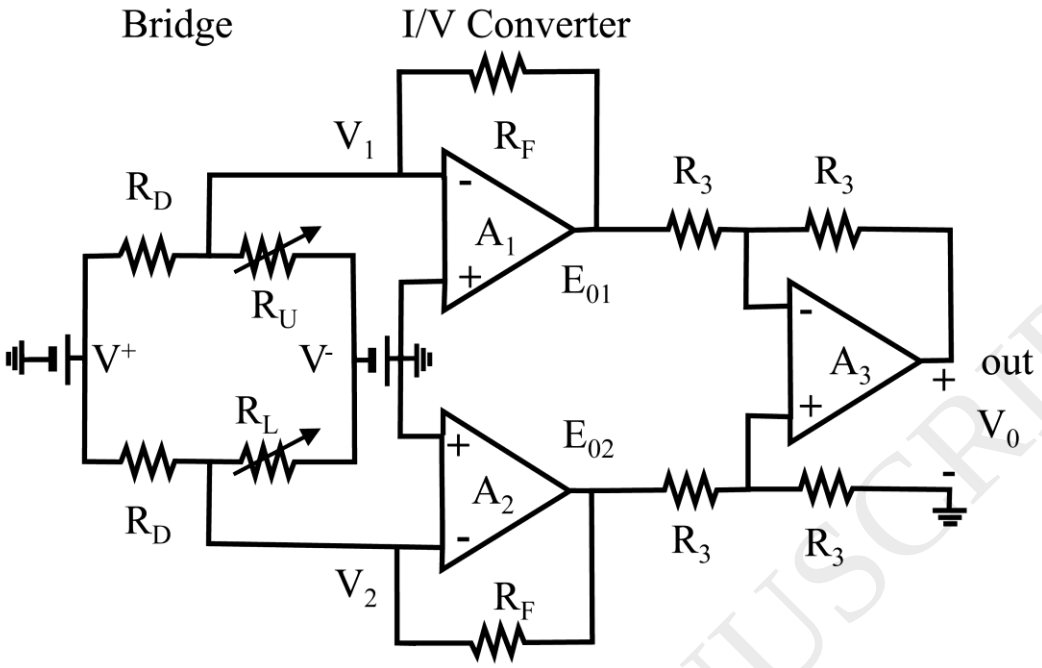

Figure 18

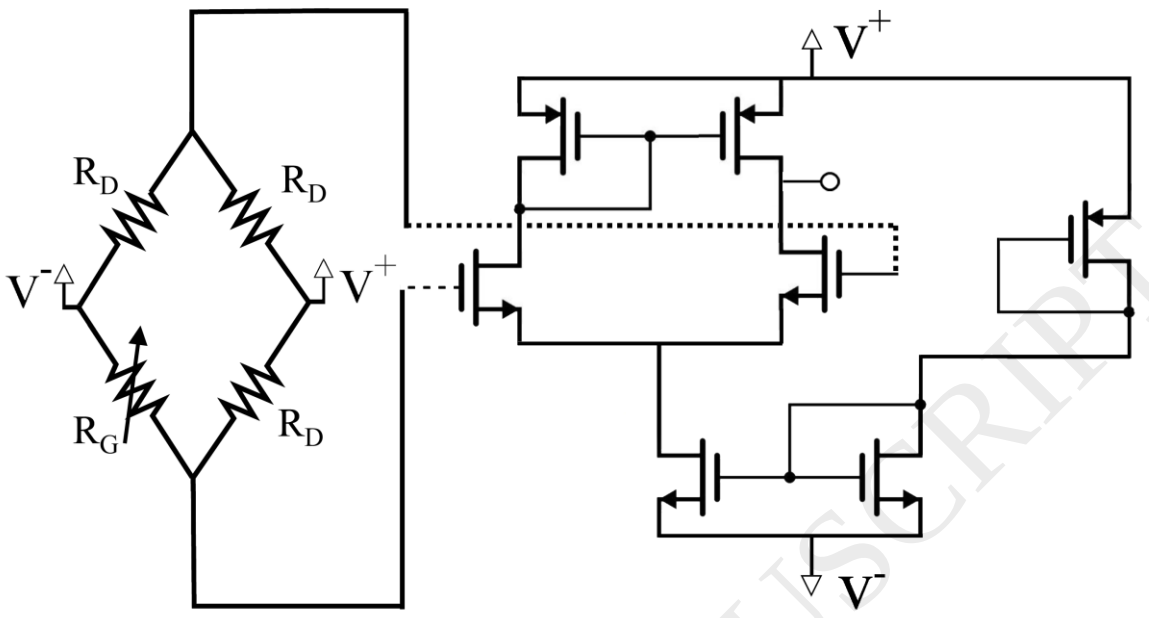

Figure 19

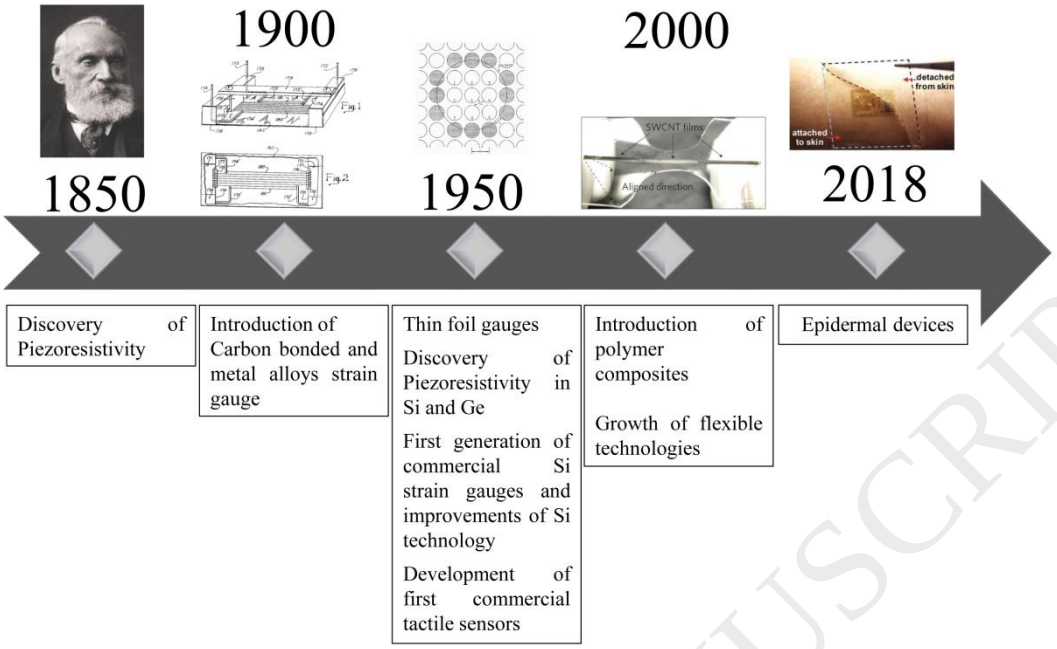

Figure 20

Table 1
Resistivity and longitudinal gauge factors of the most common metals used for piezoresistive sensors.

Material	Resistivity (20 °C) [10^{-6} Ω·cm]	GF_l	Ref.
Aluminum	2.650	3.1	[33, 30]
Copper	1.678	2.9	[33, 30]
Gold	2.214	4.48	[33, 35]
Iron	9.61	4.2	[33, 32]
Nichrome V	100	2.0	[34, 32]
Nickel	6.93	–12.2	[31, 32]
Platinum	10.5	4.8	[33, 32]
Silver (printed)	1.587	3.35±0.13	[33, 29]

Table 2
Longitudinal gauge factors of the most common semiconductor materials.

Material	GF_l			Ref.
	Silicon			
	[111]	[110]	[100]	
p–Si	175	120	8.6	[42, 51, 52]
n–Si	–135	–61.4	–133	[42, 51, 52]
p–Ge	105	65	–10.9	[30, 42]
n–Ge	–155	–105	–5.3	[30, 42]
n–GaAs	–8.9	–6.7	–3.2	[30]
	Polysilicon			
random n–Si	–82.1			[52]
random p–Si	87.5			[52]
	Silicon Carbide			
n–6H–SiC	–29.4			[40]
p–6H–SiC	27			[40]

Table 3
Resistivity of a few representative polymer conductive composites.

Material	Resistivity [Ω·cm]	Wt %	Ref.
Carbon Black/Silicone	10^5	5	[82]
SWNT/PMMA	10^3	2	[89]
MWCNT/PDMS	10^5	5	[84]
Graphene/Polystyrene	10^4	2	[88]
Expanded Graphite/PMMA	10^5	1	[90]
Expanded Graphite/Epoxy	10^6	3	[90]
Polyethylene terephthalate/graphene	~10^3	0.47	[92]

Table 4
Tactile sensor parameters.

		Ref.
Articulator design	Single/multi finger, hand–like	[120, 123]
Force	Range , direction (e.g. normal, tangential)	[124]
Resolution	Temporal (typ. 1 ms), spatial (1–5 mm)	[123]
Static characteristics	Linearity, Hysteresis (<5 %)	[123]
Dynamic characteristics	Dynamic range (1000:1), bandwidth (100 Hz or more)	[122, 124]
Material properties	Flexibility, compliance, conductive mechanisms, thermal stability	[123, 125]

Table 5
Displacement piezoresistive sensors.

Type	Material	Displacement	Force	Size	Ref.
B	Silicon	4–11 mm	1 N	11 x 11 mm^2	[129]
B	SWNT	30/40 nm	≈50 nN	200 nm^2	[135]
C	n+ $Al_{0.4}Ga_{0.6}As$	10 pm $Hz^{-1/2}$		400 x 160 μm^2	[136]
C	Cr–Ni	200 μm	74 mV/μm	24 x 24 mm^2	[137]

B: Beam, C: Cantilever.

Table 6
Flow Sensor parameters.

Size [μm^2]	Flow Range [m/s]	Material	Sensitivity [$\Omega \cdot m^{-1} \cdot s^{-1}$]	Response time [s]	Ref.
4000 x 400	5–45	Pt	0.0134 (A)	1.38	[155]
4000 x 1200	5–45	Pt	0.0227 (A)	0.99	[155]
4000 x 2000	5–45	Pt	0.0284 (A)	0.53	[155]
20 x 90	0–65	p–SiNW	198 (A)	–	[156]
400 x 1100	0.2–0.95	p–Si	4573.9 (W)	–	[151]
1500 x 400	0–17	Elastomer	66 (A)	–	[157]

A: Air, W: Water.

Table 7
Wheatstone bridge configurations.

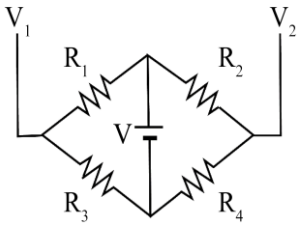

Configuration	Elements	Output Voltage
1 varying element	$R_4=R+\Delta R$ $R_1, R_2, R_3=R$	$V/4\cdot(\Delta R/(R+\Delta R/2))$
2 varying elements	$R_1=R_4=R+\Delta R$ $R_2, R_3=R$	$V/2\cdot(\Delta R/(R+\Delta R/2))$
	$R_2=R-\Delta R$; $R_4=R+\Delta R$ $R_1, R_3=R$	$V/2\cdot(\Delta R/R)$
4 varying elements	$R_1= R_4=R+\Delta R$ $R_2=R_3=R-\Delta R$	$V\cdot(\Delta R/R)$

Table 8
CMOS readout interface for piezoresistive sensors.

Type	Sensitivity	Power	Dimension	Process	Ref.
Pressure	8.9 mV/psi	3 μW	4 x 4 mm^2	0.35 μm	[187]
Pressure	4.8 mV/psi	300 μW	4 x 4 mm^2	0.35 μm	[188]
Pressure	159.5 mV/V/bar			0.13 μm	[189]
Pressure	18μV/ V/mbar	200 μW	1x1.2 mm^2	0.35 μm	[190]
Pressure	450 μV/ V/mbar		0.2 x 0.2 mm^2		[191]

Table 9
Summary Table

Material	Design	Application	Sensitivity	Other characteristics	Note	Ref
Metal alloy	Circular Ultra–thin film	Tactile Sensors for Hand Exoskeletons	0.76–4.18 μs/bar	Hysteresis 12–108 ns	Commercially available FSR	[7]
Cr/Au	Thick film Cruciform cantilever	Tactile force, shear stress, fluid flow	0.03 V/μN	Resolution 1 μN	Optically transparent Three–axis force sensor	[113]
NiCr	Beam	Tactile sensor (force and curvature)	curvature, force and deflection 40 ppm·m, 340 ppm/nN and 230 ppm/μm		e–skin on flexible substrate	[114]
$Zr_{55}Cu_{30}Ni_5Al_{10}$ metallic glass	Thin–film layer	Tactile sensor	–	GF ≅2.86 Electric conductivity ≅5 10^3 Scm^{-1}	Flexible substrate Light transmittances from 0.2 % to 54 % High time stability	[115]
Graphene	Cylindrical thick film	Accelerometer	2.6 mV/g	Bandwidth: 20–300 Hz	Use as accelerometer as well as microphone	[70]
PDMS/Graphene Nano–platelets	Cylindrical thick film	Pressure sensor	0.23 kPa^{-1}	Max Pressure: 70 kPa	PDMS foam coated with conductive micro–platelets	[72]
Polyethylenimine/Graphene Oxide	Ultra–thin film	Strain sensor	–	GF 754 (ε=5 %) Resolution 0.1 % Maximum strain up to 50 % Response time: 0.6 s	Detection of motion of human knuckles	[73]
CNT/PDMS	Double spiral	Tactile sensor	–	Strain: up to 60 % High sensitivity up to 1 N	Sensitivity can be enhanced by controlling the content of CNT and porosity of CNT–PDMS	[77]
SWCNT/PDMS	Thin film	Strain sensor	–	Measurable strain up to 280 %	Human–motion detection	[78]

				Durability: 10,000 strain cycles Linear up to 150 % strain GF: 0.82		
Carbon Black/silicone	Thick film	Pressure sensor		Critical Pressure of 12 MPa GF of about 35 at low strain	Application in electronic skin	[82]
SOI	Diaphragm	Pressure Sensor	71 mV/bar	Pressure range: 0–10 bar Maximum nonlinearity of 0.2 %		[141]
Polysilicon	Diaphragm	Pressure sensor	3.35–3.74 mV/bar	Pressure range: 0–30 bar Linearity: <0.3 % full scale Hysteresis: <0.1 % full scale		[145]
SiNWs	Cantilever	Flow sensor	198 Ω/m/s	Linearity: <0.1 % Power consumption: 1 μW		[156]